

Abstract

The chemical composition of particulate matter samples (TSP, PM₁₀ and PM_{2.5}) collected from 2002 to 2008 in the North Atlantic free troposphere at Izaña Global Atmospheric Watch (GAW) observatory (Tenerife, The Canary Islands) was studied. The analysis of the samples collected in the Saharan Air Layer (SAL) shows that soil desert dust is very frequently mixed with particulate pollutants. An analysis of this data set with Median Concentrations At Receptor (MCAR) plots allowed to identify the potential source regions of the dust and particulate pollutants. Areas located at the south of the Southern slope of Atlas emerge as the most frequent source of the soil desert dust advected to the northern edge of the SAL in summer. Industrial emissions occurring along the Atlantic coast of Morocco, Northern Algeria, Eastern Algeria and Tunisia appear as the most important source of the nitrate, ammonium and a fraction of sulphate (at least a 60% of the sulphate <10 µm transported from some regions) observed in the SAL. These emissions are mostly linked to crude oil refineries, phosphate-based fertilizer industry and power plants. Although desert dust emissions appear as the most frequent source of the phosphorous observed in the SAL, high P concentrations are observed when the SAL is affected by emissions from open mines of phosphate and phosphate based fertilizer industry. The results also show that a significant fraction of the sulphate (up to 90% of sulphate <10 µm transported from some regions) observed in the SAL is linked to soil emissions of evaporite minerals in well defined regions where dry saline lakes (chotts) are present. These interpretations of the MCAR plots are consistent with the results obtained with the Positive Matrix Factorization receptor modelling. The results of this study show that North African industrial pollutants may be mixed with desert dust and exported to the North Atlantic in the Saharan Air Layer.

ACPD

11, 8841–8892, 2011

Transport of dust and pollutants mixings

S. Rodríguez et al.

Title Page

Abstract

Introduction

Conclusions

References

Tables

Figures

◀

▶

◀

▶

Back

Close

Full Screen / Esc

Printer-friendly Version

Interactive Discussion



1 Introduction

Desert regions of Northern Africa are the largest source of soil dust suspended in the atmosphere of the Earth. It is estimated that annual emissions range within the interval 300–1600 Tg/y. They account for 60–70% of global desert dust emissions and they are 2–3 times larger than those of the Asian deserts, the second most important dust source region (Ginoux et al., 2004; Engelstaedter et al., 2006).

Dust plays an important role in processes affecting climate, biogeochemistry and air quality. Very briefly, the presence of dust influences on the energy distribution in the atmosphere, owing to it scatters and absorbs radiation (Haywood et al., 2003).

Moreover, dust particles may act as cloud condensation nuclei and consequently they influence on rain and on cloud radiative properties (Levin et al., 1996). Some trace elements of dust participate in marine biogeochemical processes: the rate production of nitrate and ammonium of some cyanobacterias that utilize iron in their metabolism may be controlled by dust deposition in the ocean (Michaels et al., 1996); moreover, the Fe and P supplied by dust deposition on “high nutrient, low chlorophyll oceanic regions” may be a limiting factor for nitrogen fixation by phytoplankton (Falkowski et al., 1998; Mills et al., 2004). In consequence, dust deposition may modulate the carbon cycle. Finally, dust may also affect air quality. In urban areas affected by advections of Saharan dust, an increase in mortality (Pérez et al., 2008; Jiménez et al., 2010) and in cardiovascular diseases (Middelton et al., 2008) has been observed.

Regional dust production and exportation in North Africa experience a marked seasonal evolution. Because of the seasonal shift of the intertropical convergence zone, the sources of soil desert dust located in Sahel are mostly activated in winter (Harmattan winds), whereas those located in northern subtropical Saharan latitudes are activated in summer (Engelstaedter et al., 2006; Sunnu et al., 2008). Thus, the so-called Saharan Air Layer (SAL) is westward exported at low “tropical” latitudes (<15° N) in winter and at higher “subtropical” latitudes in summer (15–30° N). This behavior can be observed in Fig. 1, where the Aerosol Index (AI) averaged for January and July

Transport of dust and pollutants mixings

S. Rodríguez et al.

Title Page

Abstract

Introduction

Conclusions

References

Tables

Figures

◀

▶

◀

▶

Back

Close

Full Screen / Esc

Printer-friendly Version

Interactive Discussion



is shown. AI is sensitive to the presence of UV-absorbing aerosols above 1 km a.s.l., including mineral dust (Torres et al., 1998).

Although soil dust emissions are, by far, the most important source of the particles present in the SAL, there is an increasing number of evidences pointing that anthropogenic activity may be prompting changes in the amount and composition of the particles present in the SAL. Three examples:

- Dust particles exported in the winter tropical SAL (Fig. 1b) are often externally mixed with carbonaceous and inorganic trace species (e.g. K^+) linked to biomass burning in Sahel during the dry season (Formenti et al., 2003; Capes et al., 2008).
- A number of observations have shown that soil dust in the SAL is very often mixed with sulphate and nitrate; e.g. observations in the Canary Islands (Prospero et al., 1995; Alastuey et al., 2005; Kandler et al., 2007), Cape Verde (Formenti et al., 2003; Dall'Osto et al., 2010) and Caribbean (Reid et al., 2003). The few studies focused on investigating the origin of these pollutants have shown that the transport of pollutants from Europe and their mixing with North African desert dust may contribute to the observed dust-pollutants mixing (Millán et al., 1997; Kallos et al., 1998; Gangoiti et al., 2006; Astitha et al., 2010).
- There are huge uncertainties on how human activities are changing soil dust emissions. Zender et al. (2004) defined anthropogenic soil dust as that part of the dust load that is produced by human activity. This may occur by two ways: (1) by land use which changes soil surface conditions that modify the potential for soil dust emission (e.g. by agriculture, mining, livestock, vehicles or water management), and (2) by modifying climate, which in turn modifies dust emissions, for example, by changes in surface winds or vegetation growth.

The objective of this study is to investigate the origin of some aerosol species observed in the SAL that may be influenced by anthropogenic activities. We focus part of our attention on nitrate, ammonium and sulphate. The mixing of these species with

Transport of dust and pollutants mixings

S. Rodríguez et al.

Title Page

Abstract

Introduction

Conclusions

References

Tables

Figures

◀

▶

◀

▶

Back

Close

Full Screen / Esc

Printer-friendly Version

Interactive Discussion



dust may prompt changes in the physical properties of the SAL and this may have important consequences in processes affecting climate. For example, the coating of the dust particles (Dentener et al., 1996) with these species may enhance the hygroscopic properties and light scattering efficiency of the SAL particles (Levin et al., 1996; Astitha et al., 2010).

2 Methods

2.1 Sampling site

This study is based on aerosol data collected at Izaña “Global Atmospheric Watch” (GAW) observatory (16° 29′ 58″ W; 28° 18′ 32″ N; <http://www.aemet.izana.org>). This is a global important research site located in Tenerife (Canary Islands) at 2367 m a.s.l. (m a.s.l.), above the mantle of stratocumulus typically present on the top of the marine boundary layer. Izaña remains within the SAL during most of summertime (its location is highlighted with red circle in Fig. 1). Measurements at this site are considered representative of the free troposphere. Details on the meteorological features may be found elsewhere (e.g. references within Rodríguez et al., 2009).

2.2 Size distribution and particulate matter sampling

Samples of total suspended particles (TSP) and particulate matter with aerodynamic diameters smaller than 10 microns (PM_{10}) and 2.5 microns ($PM_{2.5}$) were systematically collected at Izaña. We will refer to this set of parameters as PM_x . The PM_x monitoring program was based on TSP and $PM_{2.5}$ from May 2002 to December 2004, on PM_{10} and $PM_{2.5}$ since 2005. Simultaneous TSP, PM_{10} and $PM_{2.5}$ sampling is performed every summer since 2008. From 2002 to 2007 each sampling lasted 24-h. Since January 2008, the PM_x sampling is performed at night (22:00 to 06:00 UTC). PM_x concentrations were determined by gravimetry. A total of 192 TSP, 203 PM_{10} and

Title Page

Abstract

Introduction

Conclusions

References

Tables

Figures

◀

▶

◀

▶

Back

Close

Full Screen / Esc

Printer-friendly Version

Interactive Discussion



275 PM_{2.5} samples have been collected and chemically analyzed. The sampling was performed in micro quartz fiber filters pretreated by heating to 205 °C during 5 h. Filter conditioning and weighting was performed following the procedure described in the EN-14907, except for RH, which was established to 35 ± 5%. Blank field filters were also collected.

Particle size distribution was measured with an Aerodynamic Particle Sizer (APS; TSI™) and with a Scanning Mobility Particle Sizer (SMPS; TSI™). Details on the in-situ aerosol characterization program of Izaña are provided online (<http://gaw.empa.ch/gawsis/> and <http://www.aemet.izana.org/>)

2.3 Chemical characterization

Thereafter, filters were analyzed by different techniques in order to determine the concentrations of about 60 elements and components. A half of the filter was bulk acidic digested (HF:HClO₄:HNO₃), and the solution obtained was analysed for the determination of the concentrations of major and trace elements by means of Inductively Coupled Plasma Atomic Emission Spectrometry, (ICP-AES, IRIS Advantage TJA Solutions, THERMO), and Inductively Coupled Plasma Mass Spectrometry, (ICP-MS, X Series II, THERMO), respectively. A quarter of the filter was water leached for the determination of the concentrations of soluble ions by means of Ionic Chromatography HPLC (High Performance Liquid Chromatography), for Cl⁻, SO₄²⁻ and NO₃⁻, and a ion selective electrode for NH₄⁺. Total carbon (TC) concentrations were measured by using an Elemental Carbon Analyser (LECO) from 2002 to 2007. Moreover, levels of organic and elemental carbon (OC and EC) were determined, in samples collected since 2007, by a thermal-optical transmission technique (Birch and Cary, 1996) using a Sunset Laboratory OC-EC analyser. Details of the analytical procedure are given by Querol et al. (2001). Relative errors of the abovementioned analysis of major species and trace elements have been estimated as lower than 10% in all the cases (Querol et al., 2008). Indirect determinations from analytical data were obtained for: (a) CO₃²⁻, calculated from the amount of Ca not present as Ca-sulphate and Ca-nitrate,

Transport of dust and pollutants mixings

S. Rodríguez et al.

Title Page

Abstract

Introduction

Conclusions

References

Tables

Figures

◀

▶

◀

▶

Back

Close

Full Screen / Esc

Printer-friendly Version

Interactive Discussion



and the assuming this fraction of Ca is present as calcite (CaCO_3 ; $\text{CO}_3^{2-} = 1.5 \cdot \text{Ca}$); (b) SiO_2 , determined from the Al content on the basis of prior experimental equations ($\text{SiO}_2 = 3 \cdot \text{Al}_2\text{O}_3$, see Querol et al., 2001). Then, dust is calculated as the sum: $\text{Al}_2\text{O}_3 + \text{SiO}_2 + \text{Fe} + \text{CaCO}_3 + \text{K} + \text{Na} + \text{P} + \text{Ti} + \text{Sr}$. Blank field filters were also chemically analysed.

2.4 Source regions of dust and other aerosol species

The potential source regions of dust and of other aerosol species (e.g. sulphate or nitrate) were identified by analyzing the “Median Concentrations At Receptor (MCAR)” plots determined for each aerosol species analyzed at Izaña. These MCAR plots represent the median concentrations, recorded at Izaña, of a given aerosol compound when air masses passed above each $1^\circ \times 1^\circ$ degree pixel shown in the lat x lon grid.; e.g. Fig. 10a shows the MCAR map for nitrate.

MCAR plots were determined using five days back-trajectories calculated at 00:00 UTC using the HYSPLIT software (Draxler and Rolph, 2010) and $50 \text{ km} \times 50 \text{ km}$ ECMWF data. MCAR plots for each aerosol compound were determined by the following steps programmed in a Matlab™ script: (1) a 3-D matrix was built, where X, Y and Z dimensions correspond to lon, lat and the number back trajectories to be included in the analysis; (2) for each Z value (i.e. a given back-trajectory for a specific day) the lat lon points (i.e. X-Y elements of the 2-D matrix) intersected by the trajectory were set to the value of the concentration of the aerosol specie “A” recorded at Izaña; being the remaining elements of the 2-D matrix (X–Y) set to null; and (3) once all Z layers have been set, the median and mean of each vector Z (i.e. fixed lat-lon, X–Y, point) were determined and then plotted (e.g. Figs. 8, 10 and 14).

MCAR plots were determined for each aerosol compound analyzed in PM_{10} (2005–2008). High concentrations of a given aerosol compound on a specific region of the MCAR plot may be caused by two possible processes: (1) significant emissions or formation rates of that aerosol specie in that area, (2) air masses that pass over that region are usually enriched in that aerosol species due to transport from upwind areas.

Transport of dust and pollutants mixings

S. Rodríguez et al.

Title Page

Abstract

Introduction

Conclusions

References

Tables

Figures

◀

▶

◀

▶

Back

Close

Full Screen / Esc

Printer-friendly Version

Interactive Discussion



In order to differentiate these two scenarios, the MCAR plots were interpreted using a number of information sources described below.

2.5 Sources of information

MCAR plots were interpreted using a wide variety of sources. The location and nature of mining and industrial activities were identified using the Mineral Yearbooks of the US Geological Survey (Newman, 2008; Taib, 2008a; 2008b) and online information on power plants, refineries and chemical plants (e.g. www.mining-technology.com, www-wds.worldbank.org, www.wikipedia.com or www.afribiz.info). These sources were then identified and located in Google Earth™ and Google Map™. Similarly, the geographical and geomorphologic features of the observed source regions of dust were characterised using Atlases and Google Earth™ and Google Map™. Table 1 and Fig. 2 provide the location and information about the industrial sources and mining areas. The coordinates of the identified sources of dust and other aerosols is provided in order the reader may use Google Earth™ and Google Map™ for having a satellite view. In many cases, Google Earth™ includes a link to pictures performed in-situ and available in Panoramio™ (www.panoramio.com).

2.6 Positive matrix factorization

The identification of the profile of the potential sources contributing to PM₁₀ levels and composition at Izaña was identified by analyzing the PM₁₀ composition data set with the Positive Matrix Factorization model, version 2 (PMF2; Paatero, 1997). PMF model is a factor analytical tool that provides the profile and contribution of the identified sources to each aerosol constituent (Paatero and Tapper 1994; Paatero 1997). The model is based on the weighted least-squares method, in such a way that individual estimation of the uncertainty in each data value are needed and included in the model. In the present study, individual uncertainties were calculated as in Amato et al. (2009), taking into accounts the analytical uncertainties as well as the standard deviations of species

Transport of dust and pollutants mixings

S. Rodríguez et al.

Title Page

Abstract

Introduction

Conclusions

References

Tables

Figures

◀

▶

◀

▶

Back

Close

Full Screen / Esc

Printer-friendly Version

Interactive Discussion



concentrations in the blank filters. The number of species used within the PMF model was selected by looking at their signal-to-noise ratio (S/N) and, as proposed by Paatero and Hopke (2003), only species with S/N values higher than 2 were selected for the present study. Moreover, PMF2 was run in robust mode (Paatero, 1997), and rotational ambiguity was handled by means of the FPEAK parameter (Paatero et al., 2005).

3 Results

3.1 Particulate matter composition

Figure 3a shows concentrations of aluminum and of bulk PM_{10} recorded at Izaña. Al is included as soil dust tracer (clay mineral). Concentrations of PM_{10} experience a large variability. During non dusty conditions PM_{10} typically shows concentrations within the range $1\text{--}5\ \mu\text{g}/\text{m}^3$. This is the predominant situation during most of the year: “clean free troposphere” conditions. The simultaneous increases in PM_{10} and in Al concentrations registered at Izaña indicates that increases in the aerosol mass above the clean free troposphere background are prompted by the advectations of Saharan dust, when PM_{10} may reach values as high as $150\ \mu\text{g}/\text{m}^3$ (as 8-h or 24-h average). Other chemical compounds, such as Ca, Fe, K, Mg, V, Ni, La, Co, Cr or As, exhibits a time evolution similar to those observed in Al (not shown graphically). Observe in Table 2 how all compounds analyzed in PM_{10} exhibits a moderate to high correlation with Al.

We compared the chemical profile of dust we obtained at Izaña (ratios to Al, Table 3) with that observed in Saharan dust samples collected in previous studies performed at Izaña (Kandler et al., 2007), Niger (Formenti et al., 2008), Cape Verde (Formenti et al., 2003) and Puerto Rico (Reid et al., 2003). Our observations are very similar to those previous observations at those sites. The overall data analysis shows that the Fe/Al and K/Al, Mg/Al and Ca/Al ratios exhibit a relatively low variability, with average values of 0.55 ± 0.03 , 0.21 ± 0.01 , 0.18 ± 0.03 and 0.41 ± 0.08 , respectively. Unfortunately, no sulphate and nitrate ratios to Al were found in the literature to be compared with those

[Title Page](#)[Abstract](#)[Introduction](#)[Conclusions](#)[References](#)[Tables](#)[Figures](#)[◀](#)[▶](#)[◀](#)[▶](#)[Back](#)[Close](#)[Full Screen / Esc](#)[Printer-friendly Version](#)[Interactive Discussion](#)

we found.

Sulphate and nitrate in the PM_{10} fraction exhibited a behavior similar to that of bulk PM_{10} concentrations: low concentrations under clean free troposphere conditions and high levels during dust events (Fig. 3b and 3c). The behavior we have described for PM_{10} is also observed in TSP and $PM_{2.5}$. High concentrations of TSP and $PM_{2.5}$, and sulphate and nitrate contained in these particle cut-sizes, are also recorded within the Saharan Air Layer, with daily mean concentrations of up to $700 \mu\text{g m}^{-3}$ of TSP and of $120 \mu\text{g m}^{-3}$ of $PM_{2.5}$ were measured (not shown for the sake of brevity). In fact, SO_4^- and Al showed a significant positive correlation in the three PM_x fractions (Fig. 4b and c).

Table 4a shows the mean composition of TSP, PM_{10} and $PM_{2.5}$ during events in which these parameters showed bulk mass concentration data within the percentile intervals 1–10-th, 55–85-th and 85–99-th, representative of clean free troposphere, moderate dust events and intense dust conditions, respectively. The increase in dust concentrations throughout the sequence clean free troposphere, moderate dust and intense dust conditions (e.g. ~ 0.4 , 19 and $70 \mu\text{g m}^{-3}$ in PM_{10}) is associated with an increase in the absolute concentrations of sulphate (e.g. ~ 0.3 , 1.2 and $2.4 \mu\text{g m}^{-3}$ in PM_{10}), nitrate (e.g. ~ 0.1 , 0.6 and $1.2 \mu\text{g m}^{-3}$ in PM_{10}) and ammonium (e.g. 0.06, 0.1 and $0.3 \mu\text{g m}^{-3}$ in PM_{10}), although a decrease in their relative contribution (%) to PM_x is observed. During dust events, sulphate, nitrate and ammonium accounted for 2–6%, 1–2% and 0.1–0.6% of bulk PM_x , respectively. Organic matter and elemental carbon (e.g. 1.6, 2.9 and $3.8 \mu\text{g m}^{-3}$ in PM_{10}) also showed a clear increase during dust events, however their behavior and sources will not be discussed here. Finally, the much higher correlation of Cl^- with Al than with Na evidences a low influence of sea salt (as already described by Putaud et al., 2000).

Figure 4a1–4a3 show the concentrations of sulphate versus ammonium expressed in equivalents. A clear excess of SO_4^- with respect to NH_4^+ is observed in the three PM_x size fractions (slopes > 1). This indicates that, in addition to ammonium-sulphate, other SO_4^- salts are present in the Izaña samples (e.g. calcium, magnesium or sodium

Transport of dust and pollutants mixings

S. Rodríguez et al.

Title Page

Abstract

Introduction

Conclusions

References

Tables

Figures

◀

▶

◀

▶

Back

Close

Full Screen / Esc

Printer-friendly Version

Interactive Discussion



5 sulphate). The SO_4^- vs. NH_4^+ dots close to the 1:1 line represent samples in which sulphate is predominantly present as ammonium-sulphate (AS). Dots above this line indicate the presence of non-ammonium sulphate (NAS) salts. The distribution of SO_4^- between AS and NAS species was estimated (Table 4b). Sulphate in the clean free troposphere is predominantly present as AS (~70%). However, this AS salt only accounts for about 20–36% of SO_4^- in TSP, for 28–30% of SO_4^- in PM_{10} and for 37–56% SO_4^- in $\text{PM}_{2.5}$ during dust events. Because the poor correlation between NO_3^- and NH_4^+ in the Izaña samples (not shown for the sake of brevity) and because ammonium-nitrate is typically formed under conditions not recorded at Izaña or in the Saharan airflows (low temperature and/or high relative humidity conditions; Schaap et al., 2002), we do not consider a significant presence of ammonium-nitrate. The presence of nitrate is attributed to Ca-nitrate formation in the dusty air masses (Li and Shao, 2009).

3.2 Particle size distribution

15 Table 5 shows the mass size distribution of the studied elements and compounds among three fractions: fine (<2.5 μm), coarse (2.5–10 μm) and super-coarse (>10 μm). As expected, most of the elements typically associated with soil dust mostly occur in the coarse and super-coarse ranges. For example, only the 16% of most of major (Al, Fe, K, Ca) and trace (La, Ti, P, V, Mn, Sr, Co and Cr) elements occurred in the fine fraction. In contrast, most of ammonium (77%) and about half of sulphate (53%) occurred in the fine mode. For this reason the relative amount (%) of sulphate present as AS is higher in $\text{PM}_{2.5}$ than in PM_{10} and TSP. As averaged during the dust events, the amount of sulphate present as AS accounted for 24% of total SO_4^- in TSP, for 27% of SO_4^- in PM_{10} and for 40% of SO_4^- in $\text{PM}_{2.5}$. The presence of nitrate in the coarse mode and of sulphate in the coarse and super-coarse modes is attributed to Ca and to Ca, Na and Mg bearing salts, respectively (Reid et al., 2003; Kandler et al., 2007; Li and Shao 2009; Dall'Osto et al., 2010).

25 The peculiar features of sulphate at Izaña (a significant fraction in the coarse and supercoarse fractions, and a low proportion of ammonium sulphate) contrast with those

Title Page

Abstract

Introduction

Conclusions

References

Tables

Figures

◀

▶

◀

▶

Back

Close

Full Screen / Esc

Printer-friendly Version

Interactive Discussion



observed in Europe, where this salt is predominantly present as ammonium-sulphate in the fine fraction (Rodríguez et al., 2007).

Figure 5 shows the averaged volume size distribution measured during dust episodes. Two modes are clearly observed, centered at 240 nm and 3.0 μm . The fine mode is attributed to the presence of ammonium sulphate, whereas the coarse mode is predominantly due to dust. This size distribution and the features of sulphate and nitrate described above, suggests that both external (ammonium-sulphate in the fine fraction and dust in the coarse fraction) and internal (dust coated by sulphate in the coarse mode) aerosol mixing may occur in the SAL. The coarse mode of this size distribution is similar to that observed by Maring et al. (2003) within the Saharan Air Layer in campaigns performed at Izaña and Puerto Rico.

3.3 Source region and transport pathways

In order to focus our attention on the SAL, only events with dust concentrations $>10 \mu\text{g m}^{-3}$ in PM_{10} were studied. Thus, a total of 44 dust episodes were used for determining the MCAR plots (Figs. 8, 10 and 14). These events mostly occur from July to September (Fig. 6a).

3.3.1 Transport pathways of Saharan airflows

The frequency by which air masses passed over each $1^\circ \times 1^\circ$ pixel included in the MCAR plot is shown in Fig. 6b. The region of high frequency (≥ 50 counts) reveals that there is a well defined transport pathway (red arrow in Fig. 6b): air original from the Mediterranean flows North to South across Tunisia and Northern Algeria and is then westward transported along the Southern slope of the Atlas mounts toward the North Atlantic Ocean. This transport pathway is similar to the “mean airflows” previously described by Millán et al. (1997) and Gangoiti et al. (2006). This transport pathway is the result of the meteorological scenario typical of the summertime (Fig. 7), which will be discussed below. In the frequency plot shown in Fig. 6c, the frequency scale has

Transport of dust and pollutants mixings

S. Rodríguez et al.

Title Page

Abstract

Introduction

Conclusions

References

Tables

Figures

◀

▶

◀

▶

Back

Close

Full Screen / Esc

Printer-friendly Version

Interactive Discussion



been cut to 100 in order to highlighting regions of a relatively lower frequency. It can be observed how air from other regions out of the main transport pathway may also be transported to Izaña and mixed with the SAL.

3.3.2 Aluminum

The objective of this section is to identify location of the main sources of the desert dust and to highlight the different geographical distribution with respect to the industrial sources that will be described below. The potential contribution of anthropogenic activities to Al load observed in the SAL will be discussed below (with P). A detailed description of the features of the observed soil dust sources is out of the scope of this paper. Fig. 8A shows the MCAR plot for Al. High concentrations of Al are recorded at Izaña when air masses have passed over several well delimited regions:

- Western Algeria: Bechar. A large extension of high Al concentrations is observed (in the MCAR plots) at the South of the Southern slope of Moroccan Atlas, in the so-called Bechar province in Algeria ($7\text{--}8\ \mu\text{g m}^{-3}$; centered at about 30.5°N , 3.0°W ; Figs. 2 and 8a). Maps and satellite images show a great abundance of dry drainage channels originated by water streams that flowed from the Southern slope of the Moroccan Atlas to Bechar. These drainage systems converge in many cases to wadis (the Arabic term traditionally referring to a valley which is a dry riverbed that, in many cases, contains water only during times of heavy rain or simply an intermittent stream). Some of the systems observed are the following: wadi Abadla (31.000°N , 2700°W) or wadi Bechar (31.650°N , 2.130°E). Some of them are illustrated in the map shown in Fig. 2. Many of these wadis and smaller drainage systems conclude in topographic lows where lakes may be formed during floods. Satellite images allow identifying large extensions of topographic low with appearance of beds of dry lakes, with large amounts of accumulated dust deposits (dry alluvial). Figure 9A shows, as an example, the system located at the South of the Algerian part of the wadi Ouead-Dsoura: the drainage channels and

Transport of dust and pollutants mixings

S. Rodríguez et al.

Title Page

Abstract

Introduction

Conclusions

References

Tables

Figures

◀

▶

◀

▶

Back

Close

Full Screen / Esc

Printer-friendly Version

Interactive Discussion



Transport of dust and pollutants mixings

S. Rodríguez et al.

Title Page	
Abstract	Introduction
Conclusions	References
Tables	Figures
◀	▶
◀	▶
Back	Close
Full Screen / Esc	
Printer-friendly Version	
Interactive Discussion	

the dust accumulation in the topographic low are clearly observed. In summary, large amounts of dust are accumulated along many drainage systems, wadis and topographic lows of the region (Chorowicz and Fabre, 1997). The intense NNE winds in summer favors dust emissions in this region (Fig. 7a). This is in agreement with the findings of Brooks, who, using Infra-red Difference Dust Index (IDDI) maps, observed dust emissions in this region (Brooks, 2000; Brooks and Legrand, 2000). Because of this and because Bechar is within the main transport pathway, this is probably a predominant source of the soil dust sampled at Izaña, representative of the northern side of the summer subtropical SAL.

- Northern Algeria and Tunisia. High concentrations of AI are observed (in the MCAR plots) in the southern slope of the Saharan Atlas (Fig. 8a), where a great abundance of dry drainage channels originated by water streams that flowed from the Southern Atlas toward southern lowlands are observed in Google Earth™ (also illustrated in Fig. 2). The highest concentrations of AI ($8\text{--}10\ \mu\text{g m}^{-3}$; Fig. 8a) are observed in a large topographic low that expands from Northeastern Algeria to Tunisia, where an extensive system of salt lakes and dry lakes are found. This region receives an annual direct precipitation $<100\text{ mm}$, in such a way that salt lakes have only water in the lowest area, with high amount of dust accumulated around the chotts (Prospero et al., 2002; Hamdi-Aissa et al., 2004). The largest dry salt lakes are Chott Melrhir (34.210° N , 6.360° E) in Algeria and Chott Jerid ($33\ 700^\circ\text{ N}$, 8400° E) in Tunisia. The high Aerosol Index values due to dust emissions in summer in this region (Fig. 1a) were previously described by Prospero et al. (2002).
- Eastern Algeria: Ouargla basin. An extensive area of moderate AI concentrations ($6.5\text{--}7.5\ \mu\text{g m}^{-3}$) is observed along the axis of the Ouargla basin (Figs. 2 and 8A). The axis of this basin exhibits a north-northeastward down slope. The bottom of the axis is placed at about 220 meters above the sea level on its southern edge (30.48° N , 4.28° E ; wadi Mya, descending from Northern slope of Tassili-N-Ajjer



Transport of dust and pollutants mixings

S. Rodríguez et al.

[Title Page](#)[Abstract](#)[Introduction](#)[Conclusions](#)[References](#)[Tables](#)[Figures](#)[◀](#)[▶](#)[◀](#)[▶](#)[Back](#)[Close](#)[Full Screen / Esc](#)[Printer-friendly Version](#)[Interactive Discussion](#)

mounts, located in Central Algeria) and at about 32 meters below sea level on its northern edge (in the Chott Melhrir, 34.210° N, 6.360° E, Northern Algeria). High concentrations of Al ($7\text{--}8\ \mu\text{g m}^{-3}$) are observed just in the southern part of the basin, where wady Mya descends from Tassili-N-Ajjer mount. A number of saline lakes (Chotts) lie along the axis of the basin (Fig. 12a; discussed in detail below). High Aerosol Index due to dust emissions along the Ouargla basin were previously described by Prospero et al. (2002). These were attributed to emissions of dust accumulated near the chotts. Observe in Fig. 1a how the shape of the Aerosol Index >1.5 spot over Ouargla region is similar to the topographic low of the Ouargla basin (Fig. 2).

3.3.3 Calcium

The MCAR plot for the Ca concentrations recorded at Izaña is shown in Fig. 8b. The strong northward gradient observed in Ca concentrations is in agreement with previous studies and soil maps (Schütz and Sebert, 1987; Claquin et al., 1999; Desboeufs and Cautenet, 2005; Kandler et al., 2007). These studies argued that this behavior is mainly due to the high content in calcite in the soils of Northern Morocco and Northern Algeria ($>27^\circ$ N). Hereafter we will discuss the involvement of the content of gypsum and anhydrite minerals in the soil. The potential contribution of anthropogenic activities to Ca load observed in the SAL will be discussed below (with P).

3.3.4 Nitrate, ammonium and sulphate: role of industrial emissions

Fig. 10 shows the MCAR plots for NO_3^- , NH_4^+ and SO_4^{2-} . High concentrations of these aerosol components are recorded when air arriving to Izaña have flown over the Atlantic coast of Morocco, Eastern Algeria and Northern Algeria and Tunisia. The following industrial states, emission sources of gaseous precursors (SO_x , NO_x and NH_3) of these aerosol compounds, have been identified in these regions:

– Morocco. A region of high concentrations of nitrate, sulphate and ammonium (2.0–2.2, ~0.12 and 3.0–3.5 $\mu\text{g m}^{-3}$, respectively) is observed (in the MCAR plots) parallel to the Atlantic coast of the country. The following industrial states are placed, North to South, in this region:

- Sidi Kassem (34.233° N, 5.718° W), a crude oil refinery with about ~30 000 barrels per day (bpd) production, located in the northern edge of the corridor,
- Great Casablanca area, where Mohammedia crude oil refinery (33.686° N, 7.426° W; ~125 000 bpd) and several power stations are located. Available emission inventory (dating from the early 1990s) estimated an annual SO_2 and NO_x emissions of about 94 600 and 14 800 tons/year, respectively (Khatami et al., 1998). About half of these SO_2 and NO_x emissions were attributed to Mohammedia coal fired power station (33.682° N, 7.434° W; 600 Mw),
- Jorf Lasfar, where the largest coal fired power station of the country is placed (33.105° N, 8.637° W; 1,400 Mw),
- Jorf Lasfer (33.111° N, 8.606° W) and Safi (32.222° N, 9.249° W), where two large chemical plants that produce phosphoric acid and ammonium phosphate (as part of fertilizer industry) are placed. Figure 11a and B shows a picture of Safi plant. Below it will be described how these emissions are a source of sulphate, ammonium, nitrate and other particulate pollutants in the region (CNEDD Report, 2007; Gaudry et al., 2007; Erramli et al., 2008).
- Eastern Algeria. High concentrations of nitrate, sulphate and ammonium (1.52.0, 2.5–3.5 and 0.3–0.6 $\mu\text{g m}^{-3}$, respectively) are observed in Ouargla region. This area is centered over Hassi Messahoud (31.670° N, 6.070° E), where one of the largest oil extraction field in Africa and two crude oil refineries (30 000 bpd) are placed. The plumes of these emissions around this city can be observed by the links available in Google Earth™ to Panoramio™; examples in Fig. 12c–13e.

Transport of dust and pollutants mixings

S. Rodríguez et al.

Title Page

Abstract

Introduction

Conclusions

References

Tables

Figures

◀

▶

◀

▶

Back

Close

Full Screen / Esc

Printer-friendly Version

Interactive Discussion



Transport of dust and pollutants mixings

S. Rodríguez et al.

Title Page

Abstract

Introduction

Conclusions

References

Tables

Figures

◀

▶

◀

▶

Back

Close

Full Screen / Esc

Printer-friendly Version

Interactive Discussion



The regional air quality impairment in the region to these emissions is well documented (Yassaa et al., 2001a; Yassaa and Cecinato, 2005).

- Northern Algeria and Tunisia. High nitrate, sulphate and ammonium concentrations are also observed in the coast of Algeria and Tunisia, in the Mediterranean, where the following industrial facilities are placed (Figs. 2 and 10):
 - Arzew (35.811° N, 0.265° W) crude oil refinery (60 000 bpd),
 - Algier (36.760° N, 3.066° E) crude oil refinery (60 000 bpd),
 - Skikda (36.879° N, 6.945° E) crude oil refinery (300 000 bpd),
 - Annaba (36.871° N, 7.765° E) petrochemical plant for the production of sulphuric acid, phosphoric acid and diammonium phosphate,
 - Bizerte (36.800° N, 10.290° E) crude refinery (35 000 bpd),
 - Rades (36.799° N, 10.286° E) power plant,

The air quality impairment due to the industrial emissions in these regions is a well known fact (e.g. Yassaa et al., 2001b; Ali-Khodja et al., 1998; 2008; Tlili et al., 2007).

3.3.5 Phosphorus

Relatively high phosphorous concentrations are observed (in the MCAR plots) in the Bechar basin (70–80 ng m⁻³; Fig. 8c), where important soil dust emissions occurs. Because this region is within the main transport pathway, this is probably the most frequent source of the soil P sampled at Izaña (as the case of Al discussed above). A remarkable feature is that the highest concentrations of P are observed in well defined regions where mining and industrial emissions occurs: Morocco, a “Tunisia – Eastern Algeria” SW-ward corridor and the southern slope of the Saharan Atlas (Algeria).

- Morocco. High concentrations of P (80–100 ng m⁻³) are observed in a NE to SW corridor expanding along the country (Fig. 8c). As said above, high nitrate, ammonium and sulphate concentrations (2.0–2.2, ~0.12, 3.0–3.5 µg m⁻³, respectively)

Transport of dust and pollutants mixings

S. Rodríguez et al.

[Title Page](#)[Abstract](#)[Introduction](#)[Conclusions](#)[References](#)[Tables](#)[Figures](#)[◀](#)[▶](#)[◀](#)[▶](#)[Back](#)[Close](#)[Full Screen / Esc](#)[Printer-friendly Version](#)[Interactive Discussion](#)

are also observed along this corridor (Fig. 10). The high concentrations of phosphorus and chlorine and observed along this corridor (Fig. 8c and 8e) supports the involvement of the above cited phosphate industry; e.g. that located in Safi (32.222° N, 9.249° W; Figs. 2, 11a and b) and Jorf Lasfer (33.111° N, 8.606° W; Fig. 2). Morocco is the second phosphate producer in the world, with an annual production of about 23 million tons/year. The main phosphate mines are placed in Khouribga (32.662° N, 6.703° W), Benguerir / Yousoufia (32.270° N, 7.837° W), Meskala (31.366° N, 9.477° W). Phosphate rock extractions also occur at Bou Craa in Western Sahara (26.313° N, 12.846° W). About half of ores are transformed in the above cited plants. Observe in Fig. 8c–8f and Fig. 10 how high concentrations of P, P/Al, Cl/Cl/P, NO₃⁻, SO₄⁼ and NH₄⁺ are observed in the region where the Moroccan industry and mines of phosphates are located. The emissions may occur in the mines and/or during the industrial processing (depending on the pollutant). In the mines, emissions of P containing particles may occur during the extraction process or due to the action of wind on the soil of the open mines. The change in the use of soil and soil texture due to the mining activities may increase dust emissions in the region (Zender et al., 2004). This accounts for the high concentrations of Al and Ca observed in this region of Morocco (MCAR plots in Figs. 8a–b). See an example of these mines, Benguerir/Yousoufia, in Fig. 11c. The emissions links to the industrial processing of the rock are more complex. The industrial production of phosphoric acid results from the reaction between sulphuric acid and phosphate ores. During the reaction, insoluble calcium sulphate (so called phosphogypsum) is produced. This industry results in the emissions of aerosol gaseous precursors, such as ammonia (NH₃), sulfur oxides (SO_x/SO₂), inorganic chlorine compounds (e.g. HCl and KCl), and in the emissions of primary mineral particles (e.g. calcium-sulphate and phosphate). The high ratios of P/Al and Cl/Al over the Moroccan corridor indicate enrichment in phosphorous and chloride of the dust particles in the region (Fig. 8c–f). The observed high Ca, SO₄⁼ and P concentrations agree with the main emissions of

Transport of dust and pollutants mixings

S. Rodríguez et al.

Title Page

Abstract

Introduction

Conclusions

References

Tables

Figures

◀

▶

◀

▶

Back

Close

Full Screen / Esc

Printer-friendly Version

Interactive Discussion



the region (Figs. 8 and 10). The pollution in the air, water and soils of this region of Morocco due to these industrial activities is well documented (CNEDD Report, 2007; Gaudry et al., 2007; Erramli et al., 2008). The prevailing NNE trade winds in the region (Fig. 7a) contribute to result in the plume like shape of the corridor of phosphate industry pollutants (Figs. 8 and 10).

- “Tunisia and Eastern Algeria”. High concentrations of P are observed in the MCAR plot (Fig. 8c) in the Northern part of the border between Algeria and Tunisia, in a corridor that expands from the shore southward to $\sim 32^\circ\text{N}$. This region is also significantly affected by emissions of the phosphate mines and P-based fertilizers industry. A number of open mines are distributed in the Tunisian part of the region in Gafsa province (Table 1 and Fig. 2), with rock processing plants located at: Al Mitlawi (34.340°N , 8.403°E), Umm Al Alaris (34.525°N , 8.265°E), Al Rudayyif (34.383°N , 8.145°E), Gafsa (34.290°N , 8.743°E), Jallabia, Kef Eddour, Kef Eschfaier and the Mzida. Most these open mines and processing plants are easily observed from satellite (Fig. 13a), e.g. Gafsa mine (34.290°N , 8.743°E) and Gafsa processing plant (34.310°N , 8.776°E). In 2008, Tunisia produced about 11.6Mt of raw phosphate rock, of which 879,000 t were exported, and the remaining processed in several plants of the country at Gabes (Phosphoric acid, fertilizer and ammonium nitrate production, 33.917°N , 10.093°E), M’Dhilla (Phosphoric acid and fertilizer production: 34.235°N , 8.643°E), Sfax (Phosphoric acid and fertilizer production 34.729°N , 10.776°E) and Skhira (Phosphoric acid: 34.346°N , 10.147°E). The Algerian part of the region is also affected by fertilizer industry emissions. A phosphate mine and processing rock is placed at Djebe Onk (34.705°N , 7.973°E ; Algeria), in Tébessa province. A chemical industry for the production of sulphuric acid ($\sim 5 \times 10^5 \text{ ty}^{-1}$), phosphoric acid ($\sim 1.6 \times 10^5 \text{ ty}^{-1}$), diammonium phosphate ($\sim 3.3 \times 10^5 \text{ ty}^{-1}$) is placed at Anabas (36.871°N , 7.762°E). These emissions contribute to the high NO_3^- , NH_4^+ and SO_4^{2-} concentrations observed (in the MCAR plots) in the region (Fig. 10). The impact of these emissions on the regional air

Transport of dust and pollutants mixings

S. Rodríguez et al.

[Title Page](#)[Abstract](#)[Introduction](#)[Conclusions](#)[References](#)[Tables](#)[Figures](#)[◀](#)[▶](#)[◀](#)[▶](#)[Back](#)[Close](#)[Full Screen / Esc](#)[Printer-friendly Version](#)[Interactive Discussion](#)

quality was described by Ali-Khodja et al. (1998) and Azri et al. (2007). In 2008, Algeria produced 1.8 Mt of raw phosphate, being a significant fraction obtained in this area. The fact that soils are rich in phosphate may accounts for P emissions from soils in the region simply due to wind blowing. However, the fact that large extensions of soils in the region are affected by the open mining activities indicates that part of these regional emissions may be considered as “anthropogenic”. The change in the use of soil includes mines, roads, rock management activities and wastes accumulations (Fig. 13b–c). This may accounts for the high concentrations of Al also observed in this region of the Algeria–Tunisia border (MCAR plots in Figs. 8a).

A region of high P and Cl concentrations is observed along a NE to SW corridor over the Ouargla basin (Fig. 8c and 8e). As far as we know, no industrial and/or mining P activities occur in this region. Thus, these high P and Cl concentrations are attributed to transport from the Tébessa–Gafsa region (mining area) and from the Eastern coast of Tunisia (phosphate based fertilizer industrial area; Fig. 2); i.e. those high P and Cl concentrations over Ouargla evidence a transport pathway. This latter process may also contribute to the high NO_3^- , NH_4^+ , SO_4^{2-} in the region (Fig. 10).

- Central Algeria. A small region of high P concentrations ($90\text{--}110\text{ ng m}^{-3}$) in the MCAR plot (Fig. 8c) is observed in the central part of the coast of Algeria. The region, that expands southward from the shore, is located between Arzew (35.825° N ; 0.293° W), where a phosphate plant is located, and Beni saf (35.296° N , 1.338° W), where phosphate mines are placed.

3.3.6 Sources of soil sulphate

Although this study is focused on the contribution of the industrial emissions to the pollutants observed in the SAL, the role of the potential emissions of sulphate from soils (evaporites minerals) will briefly be discussed. Fig. 14 shows the MCAR plots

for AS and for NAS in terms of concentrations and their contribution to total sulphate. AS concentrations are high over the industrialized regions described above (Morocco, North Algeria, Tunisia and Eastern Algeria), where they accounts for the 60–70% of the total sulphate (Fig. 14a–c). Concentrations of NAS are high over two well define regions: Bechar (Western Algeria) and Ouargla (Eastern Algeria).

The highest NSA concentrations are recorded in Bechar basin ($3\text{--}4\ \mu\text{g m}^{-3}$). Because concentrations of ammonium and of nitrate (particulate pollutants) are very low in this region, and because, as far as we know, no industrial activities are present in the region, the high NAS concentrations in Bechar are attributed to emissions of soil sulphate in the region. This interpretation is supported by the analysis of satellite images. As stated above, Bechar region is crossed by a number of dry drainage systems and wadis that converge in topographic lows. A zoom of the satellite images over these topographic lows allow identifying textures of white crusts combined with fingerprints of water (Fig. 10b and c). This indicates that these areas have been flooded and that salts have been formed by precipitation during the evaporation of water from lakes and lagoons, resulting in the formation of evaporite minerals (e.g. calcium, magnesium and/or sodium sulphate; Hamdi-Aissa et al., 2004). Figure 10b and c shows, as example, two zooms over a topographic low located at the South of the Argelian part of wadi Ouead-Dsoura. It can clearly be observed the mixing of salts and dust (alluvial deposits) in the dry lakes. The fact that the MCAR plot for Ca also shows high concentrations in Bechar province supports the involvement of gypsum and/or anhydrite in the region (Fig. 8b). The presence of gypsum in dust samples is described in previous mineralogical studies performed at Izaa (Alastuey et al., 2005; Kandler et al., 2007).

Concentrations of NAS are relatively high in Ouargla (Eastern Algeria): $\sim 2\ \mu\text{g m}^{-3}$ in North and of $2.0\text{--}2.5\ \mu\text{g m}^{-3}$ in the South of the basin. Our results suggest that NAS in this region may be affected both by soil and by industrial emissions. A number of saline lakes lie along the axis of this basin, more specifically in the lowest (northern) part of the basin (Fig. 12a): Chott Aïn El Beïda ($31.966^\circ\text{ N}, 5.372^\circ\text{ E}$), Chott Oum El Raned ($32.040^\circ\text{ N}, 5.380^\circ\text{ E}$), Chott Felrhir ($34.070^\circ\text{ N}, 6.050^\circ\text{ E}$), Chott Merouane ($34.136^\circ\text{ N},$

Transport of dust and pollutants mixings

S. Rodríguez et al.

Title Page

Abstract

Introduction

Conclusions

References

Tables

Figures

◀

▶

◀

▶

Back

Close

Full Screen / Esc

Printer-friendly Version

Interactive Discussion



5.936° E) or Chott Melrhir (34.210° N, 6.360° E). Moreover, dry chotts are also observed in the upper side (southern) of the basin (white spots in Fig. 12a). Studies performed in the region have described how the dust particles of clay-quartzite are accumulated and mixed with the salts around these chotts (Rezagi, 1993; Valles et al., 1997; Hamdi-Aissa et al., 2004). Google Earth™ includes links to a number of in-situ pictures where the crusts of salts are clearly observed (e.g. Fig. 12b). Although soils emissions may account for the high sulphate concentrations in Ouargla, the role of the industrial emissions in Hassi Measoud and the transport of pollutants from the North (Northern Algeria – Tunisia) should be also considered. This suggests that a fraction of NAS could be due to coating or interaction of dust particles with anthropogenic sulphate and/or their precursors (SO₂/H₂SO₄; Alastuey et al., 2005; Desboeufs and Cautenet, 2005; Dall'Osto et al., 2010). In fact, the highest NAS concentrations in Ouargla basin are observed over and downwind of Hassi Messahoud. The high Ca concentrations observed in the MCAR plot in this region points to the presence of Ca-sulphate (Fig. 8b).

3.4 Positive matrix factorization modelling

The PMF2 model was used to identify the chemical profiles of the source that contribute to PM₁₀ in the SAL. This was done for assessing the consistency of the above performed interpretations on the origin of the pollutants mixed with dust. It is important to highlight that a properly considered source apportionment is out of the scope of this study. Three potential sources affecting the levels and chemical composition of PM₁₀ were identified (Fig. 15):

1. Source 1 is traced by typical soil dust elements: Al, Ca, Fe, Mg, Mn, Ti, Rb, Sr, La and K. According to the model, this source accounts for 21.5 μg m⁻³ as averaged, i.e. 75% of bulk PM₁₀. Moreover, it accounted for 20%, 14% and 95% SO₄⁼, NO₃⁻ and Ca as average during the whole study period. The Fe/Al, K/Al, Mg/Al, Ca/Al ratios in the chemical profile of this source were 0.53, 0.20, 0.16, 0.34, respectively in good agreement with the previously reported ratios calculated from

Transport of dust and pollutants mixings

S. Rodríguez et al.

[Title Page](#)[Abstract](#)[Introduction](#)[Conclusions](#)[References](#)[Tables](#)[Figures](#)[◀](#)[▶](#)[◀](#)[▶](#)[Back](#)[Close](#)[Full Screen / Esc](#)[Printer-friendly Version](#)[Interactive Discussion](#)

Transport of dust and pollutants mixings

S. Rodríguez et al.

Title Page

Abstract

Introduction

Conclusions

References

Tables

Figures

◀

▶

◀

▶

Back

Close

Full Screen / Esc

Printer-friendly Version

Interactive Discussion



the measured ambient concentrations of these elements (Table 3).

2. Source 2: shows a profile traced by SO_4^- , Ca, Na, Mg, V, Ni, As, Pb and NO_3^- . The concentration of NH_4^+ in the chemical profile of this source is almost negligible. The profile of the source includes SO_4^- and NO_3^- , present as Ca, Na and/or Mg (only for sulphate) salts, and potential industrial tracers, such as V, Ni, As, and Pb. The presence of species potentially affected by anthropogenic emissions (e.g. SO_4^- , Ni, As, Pb) with soil dust elements (e.g. Ca, Na) suggest that this sources is related with interaction between pollutants and dust. As average during the whole study period, this source accounted for $4.3 \mu\text{g m}^{-3}$ of PM_{10} (15% of bulk mass) and for 50%, 25% and 2% of SO_4^- , NO_3^- and Ca, respectively.

3. Source 3 exhibits a chemical profile characterised by SO_4^- , NO_3^- , NH_4^+ and Cl. This profile fits with that observed in the regions where emissions from the phosphate based fertilizer industry is present: Morocco, Eastern Algeria and Tunisia (Fig. 8e, F, 10). This source accounts for the presence of ammonium sulphate $[(\text{NH}_4)_2\text{SO}_4]$ and ammonium nitrates $[\text{NH}_4\text{NO}_3]$, even if the latter is expected to be present in very low concentrations. The ratios of these compounds in the chemical profile were 0.37 and 0.34 respectively, very close to the stoichiometric ratios for ammonium sulphate and nitrate (Chow et al., 1992). This source accounted for $2.2 \mu\text{g m}^{-3}$ of PM_{10} (8% of bulk mass) and 20%, 52% and 0% of sulphate, nitrate and Ca, respectively.

The moderate to high correlation observed between the three profiles of sources, illustrated in Fig. 15(b–d), evidence that the pollutants are very well mixed with dust. Under favourable conditions, the dust + pollutants tend to result in a relatively homogeneous aerosol.

4 Summary, discussion and conclusions

Particulate matter samples (TSP, PM₁₀ and PM_{2.5}; PM_x) representative of the northern side of the summer Saharan Air Layer (SAL) were collected in the North Atlantic free troposphere at Izaña Global Atmospheric Watch observatory (Tenerife, Canary Islands). An analysis of the chemical composition of these PM_x samples shows that soil desert dust is very frequently mixed with particulate pollutants. The results of this study evidence that:

- The areas located at the south of the Southern slope of Atlas mounts are a significant source of soil dust advected toward the Atlantic in summer in the northern edge of the Saharan Air Layer.
- Emissions of the crude oil refineries, “phosphate based fertilizer industry” and power plants, located in the Atlantic coast of Morocco, Northern Algeria, Eastern Algeria and Tunisia, significantly contribute to mix desert dust with particulate pollutants such as nitrate, sulphate and ammonium. The chemical composition of PM_x and the size distribution data suggest that both internal and external mixing may occur in the aerosol population present in the SAL.
- The change in use of land and the industrial activities in some parts of North Africa may be influencing the regional dust emissions rates. This may be especially important for some compounds. A clear example is the case of phosphate. The results of this study show that, although desert dust emissions is the most important North African source of phosphorous, high P concentrations and high P/Al ratios are recorded in the SAL due to emissions in the Atlantic coast of Morocco, Tunisia and Algeria linked to phosphate mines and P-based fertilizer industry. These high emissions rates of P we have observed over these regions are in agreement with experimental observations performed by Guieu et al. (2010), who observed the highest deposition rates of P in the Mediterranean sea in the coast of Tunisia.

Title Page

Abstract

Introduction

Conclusions

References

Tables

Figures

◀

▶

◀

▶

Back

Close

Full Screen / Esc

Printer-friendly Version

Interactive Discussion



Transport of dust and pollutants mixings

S. Rodríguez et al.

[Title Page](#)[Abstract](#)[Introduction](#)[Conclusions](#)[References](#)[Tables](#)[Figures](#)[◀](#)[▶](#)[◀](#)[▶](#)[Back](#)[Close](#)[Full Screen / Esc](#)[Printer-friendly Version](#)[Interactive Discussion](#)

– Emissions of soil evaporite minerals (e.g. Ca, Mg or Na sulphate) and industrial SO_2/SO_x contribute to the sulphate concentrations typically observed in the SAL. In an attempt to quantify the contribution of North African anthropogenic activities, sulphate was segregated in two components, sulphate present as ammonium-sulphate (considered anthropogenic) and sulphate presents as non-ammonium-sulphate. This later form of sulphate is affected by both soil emissions of evaporite minerals and by coating and interaction of dust particles with sulphate and/or their precursors ($\text{SO}_2/\text{H}_2\text{SO}_4$) due to anthropogenic emissions. The highest ammonium-sulphate concentrations are observed when the SAL is mixed with pollutants emitted in industrial regions of Morocco, Eastern Algeria, Northern Algeria and Tunisia, when it accounts for 60–70% of the sulphate present in the SAL. The highest non-ammonium-sulphate concentrations are observed in regions where satellite images shows an abundance of crust of salts on topographic lows, and where salt dry lakes (chotts) are clearly observed (Bechar and Ouargla regions). In these cases, non-ammonium-sulphate accounts for 80-90% of the sulphate observed in the SAL. High non-ammonium-sulphate concentrations are also observed in regions where anthropogenic SO_2/SO_x emissions occur; there coating of dust particles by anthropogenic sulphate is expected to occur (e.g. Ouargla). Further developments are necessary for segregating the soil evaporites and the dust coating related sulphate from the non-ammonium-sulphate fraction.

The results of this and of previous studies evidence that more investigations are needed for having a comprehensive view of the processes involved in the desert dust and pollutants mixings, and their implications on the physicochemical properties of the SAL. Studies performed by Millán et al. (1997) and Gangoiti et al. (2006) have shown that aged pollutants emitted in Eastern Spain and re-circulated in the Western Mediterranean basin may also be mixed with North African desert dust, and then be exported to the North Atlantic in the SAL. These coastal and mountain breezes involved in the regional transport and aging of pollutants have also been described for the North African side of the Western Mediterranean (Algeria–Tunisia; Bouchlaghem et

al., 2007). Southward transport of particulate pollutants from urban coastal areas of Algeria to Saharan inner sites (across Atlas) was also described by Yassaa et al. (2001c). In addition to recirculation processes linked to the topographic setting in the Western Mediterranean, north-to-south corridors in the “Central Mediterranean” and in the “strait of Gibraltar–Morocco” may favour the “quick transport” pathways from Europe to North Africa (Kallos et al., 1998; Astitha et al., 2010).

Acknowledgements. This study has been carried out within the framework of the research projects GRACCIE (CSD2007-00067; Ministry of Science and Innovation of Spain), CARIATI (CGL2008-06294/CLI; Ministry of Science and Innovation of Spain), AER-REG (P07-RNM-03125; Department of Innovation, Science and Enterprise of the Government of Andalusia) and REDMAAS (CGL2009-07128-E/CLI; Ministry of Science and Innovation of Spain). We thank to NOAA Air Resources Laboratory, NOAA Earth System Research Laboratory, NASA Goddard Earth Sciences Data and Information Service Center (Giovanni service) and Google Earth™, Google map™ and Panoramio™. We recognise the excellent work performed the staff in charge of the aerosol sampling: Carlos Torres, Virgilio Varreño, Cándida Hernández, Julián Pérez, Daniel Martín, Rubén Del Campo, Cesar López, Marco Hernández, Damián Expósito, Antonio Hernández and Jose Hernández.

References

- Alastuey, A., Querol, X., Castillo, S., Escudero, M., Avila, A., Cuevas, E., Torres, C., Romero, P. M., Exposito, F., Garcia, O., Diaz, J. P., Dingenen, R. V., and Putaud, J. P.: Characterisation of TSP and PM_{2.5} at Izaña and Sta. Cruz de Tenerife (Canary Islands, Spain) during a Saharan dust episode (July 2002), *Atmos. Environ.*, 39 (26), 4715–4728, 2005.
- Amato, F., Pandolfi, M., Escrig, A., Querol, X., Alastuey, A., Pey, J., Perez, N., Hopke, P. K.: Quantifying road dust resuspension in urban environment by multilinear engine: a comparison with PMF₂, *Atmos. Environ.*, 43, 2770–2780, 2009.
- Ali-Khodja, H. and Kebabi, B.: Assessment of wet and dry deposition of SO₂ attributable to a sulphuric acid plant at Annaba, Algeria, *Environmental International*, 24, 7, 799–807, 1998.
- Ali-Khodja, H., Belaala, A., Demmane-Debbih, W., Habbas, B., and Boumagoura, N.: Air quality

Transport of dust and pollutants mixings

S. Rodríguez et al.

Title Page

Abstract

Introduction

Conclusions

References

Tables

Figures

◀

▶

◀

▶

Back

Close

Full Screen / Esc

Printer-friendly Version

Interactive Discussion



Transport of dust and pollutants mixings

S. Rodríguez et al.

Title Page

Abstract

Introduction

Conclusions

References

Tables

Figures

◀

▶

◀

▶

Back

Close

Full Screen / Esc

Printer-friendly Version

Interactive Discussion



and deposition of trace elements in Didouche Mourad, Algeria. *Environ. Monit. Assess.*, 138, 219–231, 2008.

Astitha, M., Kallos, G., Spyrou, C., O'Hirok, W., Lelieveld, J., and Denier van der Gon, H. A. C.: Modelling the chemically aged and mixed aerosols over the eastern central Atlantic Ocean - potential impacts, *Atmos. Chem. Phys.*, 10, 5797–5822, doi:10.5194/acp-10-5797-2010, 2010.

Azri, C., Medhioub, K., and Rosset, R.: Evolution of atmospheric pollutants in the city of Sfax (Tunisia) October 1996–June 1997, *Atmósfera*, 20(3), 223–246, 2007.

Birch, M. and Cary, R.: Elemental carbon-based method for monitoring occupational exposures to diesel particulate diesel exhaust, *Aerosol Sci. Technol.*, 25, 221–241, 1996.

Bouchlaghem, K., Ben Mansour, F., and Elouragin, S.: Impact of a sea breeze event on air pollution at the Eastern Tunisian Coast, *Atmos. Res.*, 86, 162–172, 2007.

Brooks, N.: Dust-climate interactions in the Sahel-Sahara zone of northern Africa, with particular reference to late twentieth century Sahelian drought, PhD thesis, Norwich Climatic Research Unit, University of East Anglia, United Kingdom, 2000.

Brooks, N. and Legrand, M.: Dust variability over northern Africa and rainfall in the Sahel, *Linking Climate Change to Land Surface Change*, edited by: McLaren, S. J. and Kniveton, D., 1–25, Kluwer Academic Publishers, 2000.

Capes, G., Johnson, B., McFiggans, G., Williams, P. I., Haywood, J., and Coe, H.: Aging of biomass burning aerosols over West Africa: Aircraft measurements of chemical composition, microphysical properties, and emission ratios, *J. Geophys. Res.*, 113, D00C15, doi:10.1029/2008JD009845, 2008.

Chorowicz, J. and Fabre, J.: Organization of drainage networks from space imagery in the Tanezrouft (Western Sahara): implications of recent intracratonic deformations, *Geomorphology*, 21, 139–151, 1997.

Chow, J. C., Watson, J. G., Lowenthal, D. H., Solomon, P. A., Magliano, K. M., Ziman, S. D., and Richards, L. W.: PM₁₀ Source Apportionment in California's San Joaquin Valley, *Atmos. Environ.*, 26A, 18, 3335–3354, 1992.

Claquin, T., Schulz, M., and Balkanski, Y.J.: Modeling the mineralogy of atmospheric dust sources, *J. Geophys. Res.*, 104(D18), 22243–22256, 1999.

CNEDD Report: Charte Nationale de l'Environnement et du Développement Durable (CNEDD), Rapport Sur La Pollution de Air, available at: <http://principal.charteenvironnement.ma/fr/pdf/publications{-}environnement/rapport{-}sur{-}la{-}pollution{-}de{-}air.pdf>, 2007.

Transport of dust and pollutants mixings

S. Rodríguez et al.

Title Page

Abstract

Introduction

Conclusions

References

Tables

Figures

◀

▶

◀

▶

Back

Close

Full Screen / Esc

Printer-friendly Version

Interactive Discussion



- Dall'Osto, M., Harrison, R. M., Highwood, E. J., O'Dowd, C., Ceburnis, D., Querol, X., and Achterberg, E. P.: Variation of the mixing state of Saharan dust particles with atmospheric transport, *Atmos. Environ.*, 44, 3135–3146, 2010.
- Desboeufs, K. V. and Cautenet, G.: Transport and mixing zone of desert dust and sulphate over Tropical Africa and the Atlantic Ocean region, *Atmos. Chem. Phys. Discuss.*, 5, 5615–5644, doi:10.5194/acpd-5-5615-2005, 2005.
- Dentener, F. J., Carmichael, G. R., Zhang, Y., Lelieveld, J., and Crutzen, P. J.: Role of mineral aerosol as a reactive surface in the global troposphere, *J. Geophys. Res.*, 101, 22869–22890, 1996.
- Draxler, R. R. and Rolph, G. D.: HYSPLIT (HYbrid Single-Particle Lagrangian Integrated Trajectory) Model access via NOAA ARL READY Website (<http://ready.arl.noaa.gov/HYSPLIT.php>), NOAA Air Resources Laboratory, Silver Spring, MD, 2010.
- Engelstaedter, S., Tegen, I., and Washington, R.: North African dust emissions and transport, *Earth Science Reviews*, 79, 73–100, 2006.
- Erramli, H., Gogon, H. D., Misdag, M. A., Sauvage, T., and Ramboz, C.: Study of pollution in the El Jadida-Safi Atlantic coastal zone (Morocco) by using PIXE and SSNTD methods, *J. Environ. Radioactiv.*, 99, 1216–1223, 2008.
- Falkowski, P. G., Barber, R. T., and Smetacek, V.: Biogeochemical controls and feedbacks on ocean primary production, *Science*, 281, 200–206, 1998.
- Formenti, P., Elbert, W., Maenhaut, W., Haywood, J., and Andreae, M. O.: Chemical composition of mineral dust aerosol during the Saharan Dust Experiment (SHADE) airborne campaign in the Cape Verde region, September 2000, *J. Geophys. Res.*, 108(D18), 8576, doi:10.1029/2002JD002648, 2003.
- Formenti, P., Rajot, J. L., Desboeufs, K., Caquineau, S., Chevaillier, S., Nava, S., Gaudichet, A., Journet, E., Triquet, S., Alfaro, S., Chiari, M., Haywood, J., Coe, H., and Highwood, E.: Regional variability of the composition of mineral dust from western Africa: Results from the AMMA SOP0/DABEX and DODO field campaigns, *J. Geophys. Res.*, 113, D00C13, doi:10.1029/2008JD009903, 2008.
- Gangoiti, G., Alonso, L., Navazo, M., García, J. A., and Millán, M. M.: North African soil dust and European pollution transport to America during the warm season: Hidden links shown by a passive tracer simulation, *J. Geophys. Res.*, 111, D10109, doi:10.1029/2005JD005941, 2006.
- Gaudry, A., Zeroual, S., Gaie-Levrel, F., Moskura, M., Boujrhah, F. Z., Cherkaoui El Moursli,

Transport of dust and pollutants mixings

S. Rodríguez et al.

Title Page

Abstract

Introduction

Conclusions

References

Tables

Figures

◀

▶

◀

▶

Back

Close

Full Screen / Esc

Printer-friendly Version

Interactive Discussion



R., Guessous, A., Mouradi, A., Givernaud, T., and Delmas, R.: Heavy metals pollution of the Atlantic Marine Environment by the Moroccan Phosphate Industry, as Observed through their bioaccumulation in *Ulva Lactuca*, *Water Air Soil Poll.*, 178, 267–285, 2007.

Ginoux, P., Prospero, J. M., Torres, O., and Chin, M.: Long-term simulation of global dust distribution with the GOCART model: correlation with North Atlantic Oscillation, *Environ. Modell. Softw.*, 19, 113–128, 2004.

Guieu, C., Loÿe-Pilot, M. D., Benyahya, L., and Dufour, A.: Spatial variability of atmospheric fluxes of metals (Al, Fe, Cd, Zn and Pb) and phosphorus over the whole Mediterranean from a one-year monitoring experiment: Biogeochemical implications, *Mar. Chem.*, 120, 164–178, 2010.

Hamdi-Aissa, B., Valles, V., Aventurier, A., and Ribolzi, O.: Soils and brine geochemistry and mineralogy of hyperarid desert playa, Ouargla basin, Algerian Sahara, *Arid Land Res. Manag.*, 18, 103–126, 2004.

Haywood, J., Francis, P., Osborne, S., Glew, M., Loeb, N., Highwood, E., Tanre, D., Myhre, G., Formenti, P., and Hirst, E.: Radiative properties and direct radiative effect of Saharan dust measured by the C-130 aircraft during SHADE: 1. Solar spectrum, *J. Geophys. Res.*, 108(D18), 8577. doi:10.1029/2002JD002687, 2003.

Jiménez, E., Linares, C., Martínez, D., and Díaz, J.: Role of Saharan dust in the relationship between particulate matter and short-term daily mortality among the elderly in Madrid (Spain), *Sci. Total Environ.*, 408(23), 5729–5736, 2010.

Kallos, G., Kotroni, V., Lagouvardos, K., and Papadopoulos, A.: On the long range transport of air pollutants from Europe to Africa, *Geophys. Res. Lett.*, 25, 619–622, 1998.

Kandler, K., Benker, N., Bundke, U., Cuevas, E., Eberta, M., Knippertz, P., Rodríguez, S., Schütz, L., and Weinbruch, S.: Chemical composition and complex refractive index of Saharan Mineral Dust at Izaña, Tenerife (Spain) derived by electron microscopy, *Atmos. Environ.*, 41, 8058–8074, 2007.

Khatami, A., Ponche, J. L., Jabry, E., and Mirabel, Ph.: The air quality management of the region of Great Casablanca (Morocco), Part 1: atmospheric emissions inventory for the year 1992, *Sci. Total. Environ.*, 209, 201–216, 1998.

Levin, Z., Ganor, E., and Gladstein, V.: The effects of desert particles coated with sulfate on rain formation in the eastern Mediterranean, *J. Appl. Meteorol.*, 35, 1511–1523, 1996.

Li, W. J. and Shao, L. Y.: Observation of nitrate coatings on atmospheric mineral dust particles, *Atmos. Chem. Phys.*, 9, 1863–1871, doi:10.5194/acp-9-1863-2009, 2009.

- Maring, H., Savoie, D. L., Izaguirre, M. A., Custals, L., and Reid, J. S.: Mineral dust aerosol size distribution change during atmospheric transport, *J. Geophys. Res.*, 108(D19), 8592, doi:10.1029/2002JD002536, 2003.
- 5 Michaels, A. F., Olson, D., Sarmineto, J. L., Ammerman, J. W., Fanning, K., Jahnke, R., Knap, A. H., Lipschultz, F., and Prospero, J. M.: Inputs, losses and transformations of nitrogen and phosphorus in the pelagic North Atlantic Ocean, *Biogeochemistry*, 35, 181–226, 1996.
- Middleton, N., Yiallourous, P., Kleanthous, S., Kolokotroni, O., Schwartz, J., Dockery, D. W., Demokritou, P., Koutrakis, P.: A 10-year time-series analysis of respiratory and cardiovascular morbidity in Nicosia, Cyprus: the effect of short-term changes in air pollution and dust storms, *Environ. Health*, 7(39), doi:10.1186/1476-069X-7-39, 2008.
- 10 Millán, M. M., Salvador, R., Mantilla, E., and Kallos, G.: Photooxidant dynamics in the western Mediterranean in summer: Results from European research projects, *J. Geophys. Res.*, 102(D7), 8811–8823, 1997.
- Mills, M. M., Ridame, C., Davey, M., La Roche, J., and Geider, R. J.: Iron and phosphorus co-limit nitrogen fixation in the eastern tropical North Atlantic, *Nature*, 429, 292–294, 2004.
- Newman, H. R.: The mineral industries of Morocco and Western Sahara, 2008 Mineral Yearbook, USGS publications, available at: <http://minerals.usgs.gov/minerals/pubs/country/africa.html#ag>, 2008.
- Paatero, P.: Least square formulation of robuste non-negative factor analysis, *Chemometr. Intell. Lab. Syst.*, 3, 23–35, 1997.
- 20 Paatero, P. and Hopke, P. K.: Discarding or downweighting high-noise variables in factor analytic models, *Anal. Chim. Acta*, 490, 277–289, 2003.
- Paatero, P. and Tapper, U.: Positive matrix factorization: a nonnegative factor model with optimal utilization of error estimates of data values, *Environmetrics*, 5, 111–126, 1994.
- 25 Paatero, P., Hopke, P. K., Begum, B. A., and Biswas, S. K.: A graphical diagnostic method for assessing the rotation in factor analytical models of atmospheric pollution, *Atmos. Environ.*, 39, 193–201, 2005.
- Pérez, L., Tobias, A., Querol, X., Künzli, N., Pey, J., Alastuey, A., Viana, M., Valero, N., González-Cabré, M., and Sunyer, J.: Coarse Particles From Saharan Dust and Daily Mortality, *Epidemiology*, 19(6), 800–807, 2008.
- 30 Prospero, J. M., Schmitt, R., Cuevas, E., Savoie, D. L., Graustein, W. C., Turekian, K. K., Volz-Thomas, A., DmHaz, A., Oltmans, S. J., and Levy II, H.: Temporal variability of summer-time ozone and aerosols in the free troposphere over the eastern North Atlantic, *Geophys. Res.*

Transport of dust and pollutants mixings

S. Rodríguez et al.

Title Page

Abstract

Introduction

Conclusions

References

Tables

Figures

◀

▶

◀

▶

Back

Close

Full Screen / Esc

Printer-friendly Version

Interactive Discussion



Transport of dust and pollutants mixings

S. Rodríguez et al.

Title Page

Abstract

Introduction

Conclusions

References

Tables

Figures

◀

▶

◀

▶

Back

Close

Full Screen / Esc

Printer-friendly Version

Interactive Discussion



Lett., 22, 2925–2928, 1995.

Prospero, J. M., Ginoux, P., Torres, O., Nicholson, S. E., and Gill, T. E.: Environmental characterization of global sources of dust with the Nimbus 7 total ozone mapping spectrometer (TOMS) absorbing aerosol product, *Rev. Geophys.*, 40(1), doi:10.1029/2000RG000095, 2002.

Putaud, J. P., Van Dingenen, R., Mangoni, M., Virkkula, A., Raes, F., Maring, H., Prospero, J. M., Swietlicki, E., Berg, O. H., Hillamo, R., and Mäkela, T.: Chemical mass closure and assessment of the origin of the submicron aerosol in the marine boundary layer and the free troposphere at Tenerife during ACE-2, *Tellus*, 52B, 141–168, 2000

Querol, X., Alastuey, A., Rodríguez, S., Plana, F., Mantilla, E., and Ruiz, C.R.: Monitoring of PM₁₀ and PM_{2.5} around primary particulate anthropogenic emission sources, *Atmos. Environ.*, 35, 845–858, 2001.

Querol, X., Pey, J., Minguillón, M. C., Pérez, N., Alastuey, A., Viana, M., Moreno, T., Bernabé, R. M., Blanco, S., Cárdenas, B., Vega, E., Sosa, G., Escalona, S., Ruiz, H., and Artíñano, B.: PM speciation and sources in Mexico during the MILAGRO-2006 Campaign, *Atmos. Chem. Phys.*, 8, 111–128, doi:10.5194/acp-8-111-2008, 2008.

Reid, E. A., Reid, J. S., Meier, M. M., Dunlap, M. R., Cliff, S. S., Broumas, A., Perry, K., and Maring, H.: Characterization of African dust transported to Puerto Rico by individual particle and size segregated bulk analysis, *J. Geophys. Res.*, 108(D19), 8591, doi:10.1029/2002JD002935, 2003.

Rezagi, M.: Dynamique des sels dans les eaux et les plantes halophytes (*Salicornia* L.) dans deux régions arides (Algérie et Espagne), Ph.D. thesis, Université d'Annaba, Algeria, 1993.

Rodríguez, S., Van Dingenen, R., Putaud, J.-P., Dell'Acqua, A., Pey, J., Querol, X., Alastuey, A., Chenery, S., Ho, K.-F., Harrison, R., Tardivo, R., Scarnato, B., and Gemelli, V.: A study on the relationship between mass concentrations, chemistry and number size distribution of urban fine aerosols in Milan, Barcelona and London, *Atmos. Chem. Phys.*, 7, 2217–2232, doi:10.5194/acp-7-2217-2007, 2007.

Rodríguez, S., González, Y., Cuevas, E., Ramos, R., Romero, P. M., Abreu-Afonso, J., and Redondas, A.: Atmospheric nanoparticle observations in the low free troposphere during upward orographic flows at Izaña Mountain Observatory, *Atmos. Chem. Phys.*, 9, 6319–6335, doi:10.5194/acp-9-6319-2009, 2009.

Schaap, M., Müller, K., and ten Brink, H. M.: Constructing the European aerosol nitrate concentration field from air quality analysed data, *Atmos. Environ.*, 36, 1323–1335, 2002.

- Schütz, L. and Sebert, M.: Mineral aerosols and source Identification, *J. Aerosol. Sci.*, 18, 1–10, 1987.
- Sunnu, A., Afeti, G., and Resch, F.: A long-term experimental study of the Saharan dust presence in West Africa, *Atmos. Res.*, 87, 13–26, 2008.
- 5 Taib, M.: The mineral industries of Algeria, 2008 Mineral Yearbook, USGS publications, available at: <http://minerals.usgs.gov/minerals/pubs/country/africa.html#ag>, 2008a.
- Taib, M.: The mineral industries of Tunisia, 2008 Mineral Yearbook, USGS publications, available at: <http://minerals.usgs.gov/minerals/pubs/country/africa.html#ag>, 2008b.
- 10 Tlili, N., Zarrouk, S., Boughediri, L., and Chaoui, F.: Bio-indication of air quality in the Annaba city (East of Algeria), *Research Journal of Biological Sciences*, 2(6), 617–619, 2007.
- Torres, O., Bhartia, P. K., Herman, J. R., Ahmad, Z., and Gleason, J.: Derivation of aerosol properties from a satellite measurements of backscattered ultraviolet radiation: Theoretical basis, *J. Geophys. Res.*, 103, 17099–17110, 1998.
- 15 Yassaa, N. and Cecinato, A.: Composition of torched crude oil organic particulate emitted by refinery and its similarity to atmospheric aerosol in the surrounding area, *Chemosphere*, 60, 660–1666, 2005.
- Yassaa, N., Meklati, B. Y., Cecinato, A., Marino, F., and Balducci, C.: Organic content of particulate matter in the atmosphere of Ouargla city, Algeria, *Ann. Chim-Rome*, 91, 577–585, 2001a.
- 20 Yassaa, N., Meklati, B. Y., and Cecinato, A.: Chemical characteristics of organic aerosols in Algiers city area: influence of a fat manufacture plant, *Atmos. Environ.*, 35, 6003–6013, 2001b.
- Yassaa, N., Meklati, Y., Brancaloni, E., Frattoni, M., and Ciccioli, P.: Polar and non-polar volatile organic compounds (VOCs) in urban Algier and Saharan sites of Algeria, *Atmos. Environ.*, 35, 787–801, 2001c.
- 25 Valles, V., Rezagui, M., Auque, L., Semadi, A., Roger, L., and Zouggar, H.: Geochemistry of saline soils in two arid zones of the Mediterranean basin. I. Geochemistry of the Chott Melghir–Mehrouane watershed in Algeria, *Arid Soil Res. Rehab.*, 11, 71–84, 1997.
- Zender, C. S., Miller, R. L., and Tegen, I.: Quantifying mineral dust mass budgets: terminology, constraints, and current estimates, *EOS, Trans. Am. Geophys. Union*, 85, 48, 509–512, 2004.
- 30

Transport of dust and pollutants mixings

S. Rodríguez et al.

Title Page

Abstract

Introduction

Conclusions

References

Tables

Figures

◀

▶

◀

▶

Back

Close

Full Screen / Esc

Printer-friendly Version

Interactive Discussion



Table 1. Location and characteristics of the main industries and phosphate mines in Morocco, Algeria and Tunisia. Ac: acronymous.

Name	Ac.	Location	Activity
SIDI KASSEM	SD	34.233° N, 5.718° W	Oil refinery, 30000 bpd
MOHAMMEDIA	MH	33.686° N, 7.426° W	Oil refinery; 125 000 bpd
MOHAMMEDIA	MH	33.682° N, 7.435° W	Coal power plant (600 Mw)
JORF LASFER	JL	33.105° N, 8.637° W	Coal power plant (1400 Mw)
JORF LASFER	JL	33.111° N, 8.606° W	Fertilizer: production of -phosphoric acid -ammonium phosphate
SAFI	SF	32.222° N, 9.249° W	Fertilizer: production of -phosphoric acid -ammonium phosphate
ARZEW	AZ	35.812° N, 0.265° W	Oil refinery (60 000 bpd), petro-chemistry and fertilizer production
ALGIER	AR	36.760° N, 3.065° E	Oil refinery (60 000 bpd)
SKIKDA	SK	36.880° N, 6.958° E	Oil refinery (30 000 bpd)
ANABAS	AN	36.871° N, 7.762° E	Fertilizer. Production of: -sulphuric acid, -phosphoric acid, -diamonium phosphate,
DJEBE ONK	DO	34.705° N, 7.973° E	phosphate rock processing
BIZERTE	BZ	37.258° N, 9.885° E	Oil refinery (35 000 bpd)
RADES	TR	36.799° N, 10.286° E	Diesel and gas power plants
SFAX	SX	34.729° N, 10.776° E	Phosphoric acid and fertilizer production
SKHIRA	SH	34.346° N, 10.147° E	Phosphoric acid
M'DHILLA	MD	34.235° N, 8.643° E	Phosphoric acid and fertilizer production
GABES	GB	33.917° N, 10.093° E	Phosphoric acid, fertilizer and ammonium nitrate production
Khouribga		32.662° N, 6.703° W	Phosphate rock mine
Benguerir/Yousoufia		32.270° N, 7.837° W	Phosphate rock mine
Meskala		31.366° N, 9.477° W	Phosphate rock mine
Djebeonk		34.705° N, 7.973° E	Phosphate rock mine
Al Mitlawi		34.390° N, 8.355° E	Phosphate rock mine
Umm Al Alaris		34.525° N, 8.265° E	Phosphate rock mine
Al Rudayyif		34.389° N, 8.250° E	Phosphate rock mine

**Transport of dust and
pollutants mixings**

S. Rodríguez et al.

Title Page

Abstract

Introduction

Conclusions

References

Tables

Figures

◀

▶

◀

▶

Back

Close

Full Screen / Esc

Printer-friendly Version

Interactive Discussion



Transport of dust and pollutants mixings

S. Rodríguez et al.

Table 2. Cross correlation matrix of PM₁₀ components at Izaña.

	PM ₁₀	Al	Fe	K	Mg	Ca	Na	Cl	SO ₄ ⁼	NO ₃ ⁻	NH ₄ ⁺	La	Ti	P	V	Mn	Sr	Co	Cr	As	Pb	Ni	
PM ₁₀	1.00																						
Al	0.98	1.00																					
Fe	0.98	0.99	0.49																				
K	0.98	0.97	0.53	1.00																			
Mg	0.98	0.96	0.54	1.00	1.00																		
Ca	0.91	0.87	0.52	0.95	0.97	1.00																	
Na	0.76	0.70	0.78	0.79	0.80	0.82	1.00																
Cl	0.65	0.61	0.41	0.68	0.69	0.71	0.68	1.00															
SO ₄ ⁼	0.91	0.89	0.53	0.93	0.93	0.91	0.80	0.66	1.00														
NO ₃ ⁻	0.71	0.75	0.31	0.68	0.68	0.55	0.44	0.50	0.71	1.00													
NH ₄ ⁺	0.40	0.42	0.07	0.36	0.36	0.28	0.16	0.41	0.44	0.62	1.00												
La	0.96	0.98	0.48	0.94	0.92	0.82	0.64	0.55	0.85	0.74	0.39	1.00											
Ti	0.98	0.99	0.48	0.96	0.95	0.85	0.67	0.58	0.87	0.75	0.41	0.99	1.00										
P	0.95	0.96	0.50	0.94	0.92	0.83	0.68	0.62	0.87	0.76	0.45	0.94	0.94	1.00									
V	0.95	0.96	0.49	0.93	0.92	0.84	0.67	0.55	0.86	0.70	0.34	0.98	0.98	0.92	1.00								
Mn	0.98	0.99	0.58	0.97	0.96	0.86	0.73	0.61	0.88	0.74	0.40	0.98	0.98	0.95	0.96	1.00							
Sr	0.96	0.93	0.53	0.98	0.99	0.98	0.82	0.68	0.93	0.63	0.29	0.89	0.89	0.89	0.91	0.92	1.00						
Co	0.96	0.95	0.71	0.95	0.95	0.89	0.84	0.62	0.89	0.65	0.29	0.93	0.93	0.90	0.92	0.96	0.93	1.00					
Cr	0.38	0.36	0.38	0.37	0.37	0.37	0.31	0.29	0.31	0.31	0.02	0.36	0.36	0.39	0.36	0.39	0.40	0.38	1.00				
As	0.95	0.93	0.54	0.96	0.97	0.94	0.78	0.65	0.91	0.63	0.31	0.90	0.90	0.87	0.91	0.92	0.96	0.93	0.41	1.00			
Pb	0.57	0.53	0.77	0.55	0.55	0.53	0.66	0.46	0.56	0.39	0.14	0.52	0.52	0.58	0.53	0.58	0.57	0.65	0.60	0.58	1.00		
Ni	0.54	0.51	1.00	0.53	0.54	0.52	0.78	0.41	0.53	0.31	0.07	0.48	0.48	0.50	0.49	0.58	0.53	0.71	0.38	0.54	0.77	1.00	

[Title Page](#)
[Abstract](#)
[Introduction](#)
[Conclusions](#)
[References](#)
[Tables](#)
[Figures](#)
[Back](#)
[Close](#)
[Full Screen / Esc](#)
[Printer-friendly Version](#)
[Interactive Discussion](#)


Title Page

Abstract

Introduction

Conclusions

References

Tables

Figures

I◀

▶I

◀

▶

Back

Close

Full Screen / Esc

Printer-friendly Version

Interactive Discussion



Table 3. Mass ratio of concentration of selected elements with respect to aluminum (X/Al) and r^2 coefficient of the X versus Al plot for several aerosol components (where X is any aerosol element/component).

	TSP Izaña*		PM ₁₀ Izaña*		PM _{2.5} Izaña*		PM ₁₋₁₀ Izaña ¹		TSP Niger ²	PM ₅ P. Rico ³	PM ₁ C. Verde ⁴
	X/Al	r^2	X/Al	r^2	X/Al	r^2	X/Al	X/Al	X/Al	X/Al	
$\mu\text{g } \mu\text{g}^{-1}$											
Si							2.14	2.70	2.13	2.18	
Fe	0.54	0.99	0.52	0.99	0.52	0.99	0.58	0.59	0.30	0.53	
K	0.23	0.98	0.21	0.96	0.23	0.96	0.20	0.20	0.17	0.21	
Mg	0.17	0.85	0.19	0.94	0.20	0.95		0.14	0.12		
Ca	0.47	0.85	0.51	0.75	0.42	0.79	0.28	0.40	0.38	0.35	
Na	0.16	0.76	0.16	0.28	0.18	0.47		0.05			
NO ₃ ⁻	0.18	0.57	0.23	0.56	0.26	0.33					
SO ₄ ²⁻	0.35	0.56	0.50	0.79	0.91	0.58			0.63		
Cl ⁻	0.11	0.56	0.16	0.37	0.16	0.11					
NH ₄ ⁺	0.04	0.15	0.06	0.13	0.17	0.09					
$\text{ng } \mu\text{g}^{-1}$											
La	0.51	0.98	0.49	0.97	0.51	0.88					
Ti	65.93	0.93	58.01	0.99	57.32	0.97		80.00	44.68		
P	12.49	0.92	11.59	0.92	12.70	0.90		12.00			
V	1.39	0.90	1.53	0.92	1.70	0.79					
Mn	9.27	0.90	9.16	0.99	8.78	0.95			5.74		
Sr	4.05	0.90	3.93	0.86	4.00	0.88					
Co	0.21	0.89	0.24	0.90	0.29	0.44			1.06		
Cr	1.38	0.82	2.23	0.13	2.63	0.09			0.85		
As	0.16	0.81	0.16	0.86	0.24	0.59					
Pb	0.57	0.76	0.95	0.28	1.58	0.28					
Ni	0.66	0.73	0.78	0.26	1.08	0.25					

*: data collected in this study. ¹⁻⁴: data collected in previous studies. ¹ Kandler et al. (2007); ²Formenti et al. (2008); ³Reid et al. (2003); ⁴Formenti et al. (2003). Ratio of major and trace elements/compounds are shown in $\mu\text{g } \mu\text{g}^{-1}$ and $\text{ng } \mu\text{g}^{-1}$, respectively.

Transport of dust and pollutants mixings

S. Rodríguez et al.

Table 4. (A) Mean composition of TSP, PM₁₀ and PM_{2.5} averaged in three intervals of PM levels: 1-th–10-th, 55-th–80-th and 85-th–99-th. (B) amount of sulphate present as ammonium-sulphate (AS: (NH₄)₂SO₄) and as non-ammonium-sulphate (NAS), expressed in μg m⁻³ and in % with respect the total of sulphate. Und: undetermined (difference between bulk PM_x concentrations and the difference of the sum of the determined compounds). ∑: sum of the determined chemical compounds.

	TSP						PM ₁₀						PM _{2.5}					
	1-th	10-th	55-th	80-th	85-th	99-th	1-th	10-th	55-th	80-th	85-th	99-th	1-th	10-th	55-th	80-th	85-th	99-th
Al:	0.0	0.2	2.0	7.5	9.7	38.2	0.0	0.0	0.6	3.9	5.1	11.7	0.0	9.0	0.4	1.5	2.0	7.9
N	23		51		27		22		51		28		31		69		39	
(A)	μg m ⁻³	%																
PM und	4.94		62.96		217.67		2.96		29.29		100.87		3.30		15.03		42.64	
∑ dust	1.05		14.53		43.53		0.59		5.28		23.28		0.58		2.26		4.59	
SO ₄ ²⁻	3.89	78.7	48.43	76.9	174.14	80.0	2.37	80.0	24.01	82.0	77.59	76.9	2.72	82.3	12.77	84.9	38.05	89.2
NO ₃ ⁻	1.37	27.7	41.72	66.3	162.08	74.5	0.39	13.1	19.24	65.7	69.93	69.3	0.25	7.5	8.36	55.6	32.20	75.5
NH ₄ ⁺	0.45	9.2	1.95	3.1	4.28	2.0	0.26	8.7	1.15	3.9	2.42	2.4	0.39	11.8	0.86	5.7	1.74	4.1
OM+EC	0.08	1.6	1.23	2.0	2.10	1.0	0.09	2.9	0.61	2.1	1.18	1.2	0.10	3.0	0.27	1.8	0.53	1.2
(B) SO ₄ ²⁻	0.13	2.6	0.26	0.4	0.29	0.1	0.06	2.1	0.13	0.5	0.26	0.3	0.10	3.0	0.18	1.2	0.24	0.6
as AS	1.86	37.7	3.27	5.2	5.40	2.5	1.57	53.1	2.88	9.8	3.81	3.8	1.88	57.0	3.10	20.6	3.35	7.8
as NAS	0.35	77	0.69	36	0.77	18	0.16	62	0.35	30	0.69	29	0.27	68	0.48	56	0.64	37
as NAS	0.10	23	1.26	64	3.51	82	0.10	38	0.80	70	1.73	71	0.12	32	0.38	44	1.10	63

[Title Page](#)
[Abstract](#)
[Introduction](#)
[Conclusions](#)
[References](#)
[Tables](#)
[Figures](#)
[◀](#)
[▶](#)
[◀](#)
[▶](#)
[Back](#)
[Close](#)
[Full Screen / Esc](#)
[Printer-friendly Version](#)
[Interactive Discussion](#)


Transport of dust and pollutants mixings

S. Rodríguez et al.

Table 5. Mass size distribution (%) of PM_x components at Izaña.

	Fine < 2.5 μm	Coarse 2.5–10 μm	Supercoarse > 10 μm
PM	0.19	0.31	0.50
Al	0.16	0.46	0.38
Fe	0.17	0.37	0.47
K	0.15	0.37	0.48
Mg	0.17	0.42	0.42
Ca	0.14	0.36	0.50
Na	0.12	0.23	0.65
Cl	0.04	0.32	0.63
SO ₄ ⁼	0.53	0.27	0.20
NO ₃ ⁻	0.20	0.71	0.10
NH ₄ ⁺	0.77	0.13	0.10
La	0.17	0.42	0.41
Ti	0.17	0.28	0.54
P	0.18	0.30	0.52
V	0.18	0.37	0.46
Mn	0.17	0.31	0.52
Sr	0.16	0.25	0.59
Co	0.17	0.41	0.42
Cr	0.17	0.32	0.50
As	0.27	0.39	0.34
Pb	0.29	0.38	0.33
Ni	0.23	0.20	0.57

Title Page

Abstract

Introduction

Conclusions

References

Tables

Figures

◀

▶

◀

▶

Back

Close

Full Screen / Esc

Printer-friendly Version

Interactive Discussion



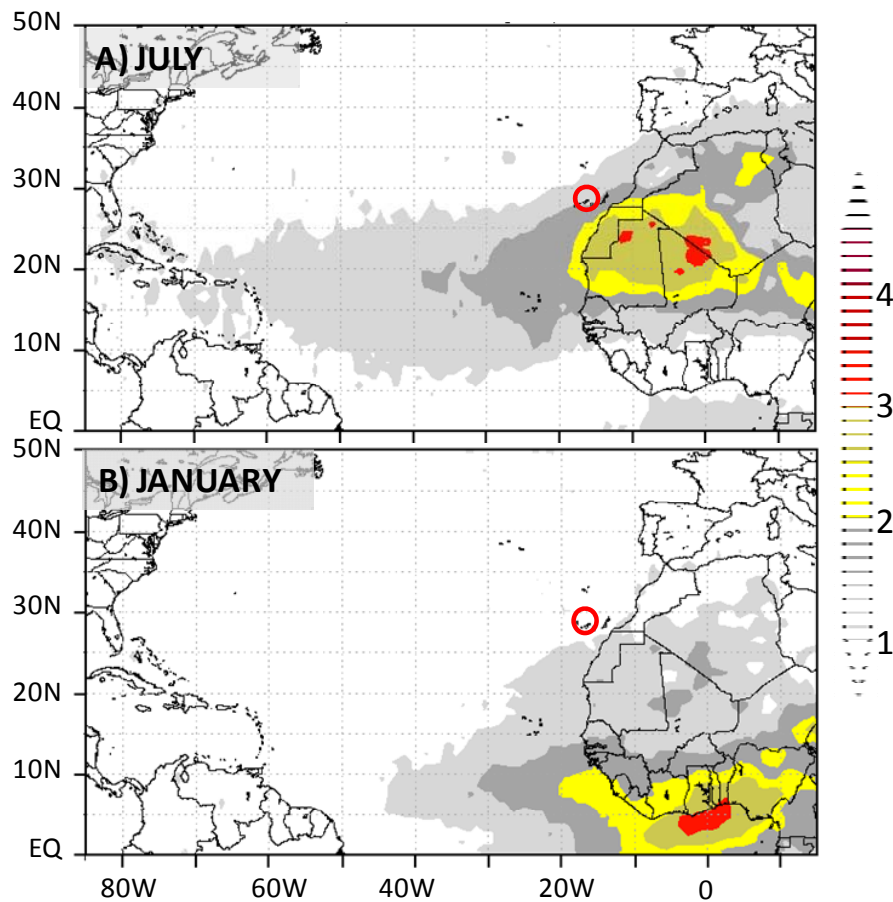


Fig. 1. Aerosol Index averaged for July and January 2008. Red circle highlights the location of Izaña.

Transport of dust and pollutants mixings

S. Rodríguez et al.

Title Page

Abstract Introduction

Conclusions References

Tables Figures

◀ ▶

◀ ▶

Back Close

Full Screen / Esc

Printer-friendly Version

Interactive Discussion



Transport of dust and pollutants mixings

S. Rodríguez et al.

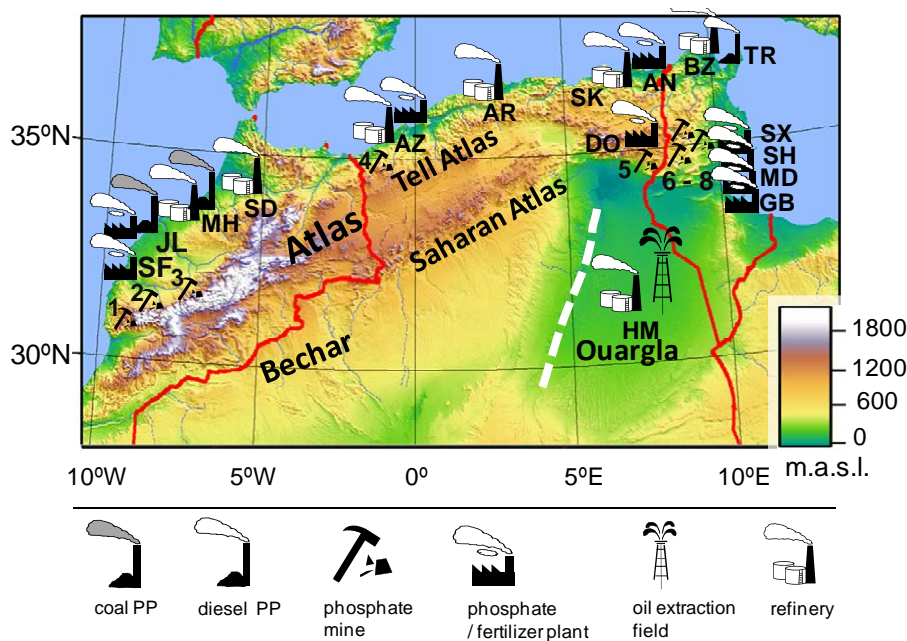


Fig. 2. Location of industrial areas and phosphate mines in Morocco, Algeria and Tunisia. PP: power plant. See Table 2 for acronyms.

Title Page	
Abstract	Introduction
Conclusions	References
Tables	Figures
◀	▶
◀	▶
Back	Close
Full Screen / Esc	
Printer-friendly Version	
Interactive Discussion	



Transport of dust and
pollutants mixings

S. Rodríguez et al.

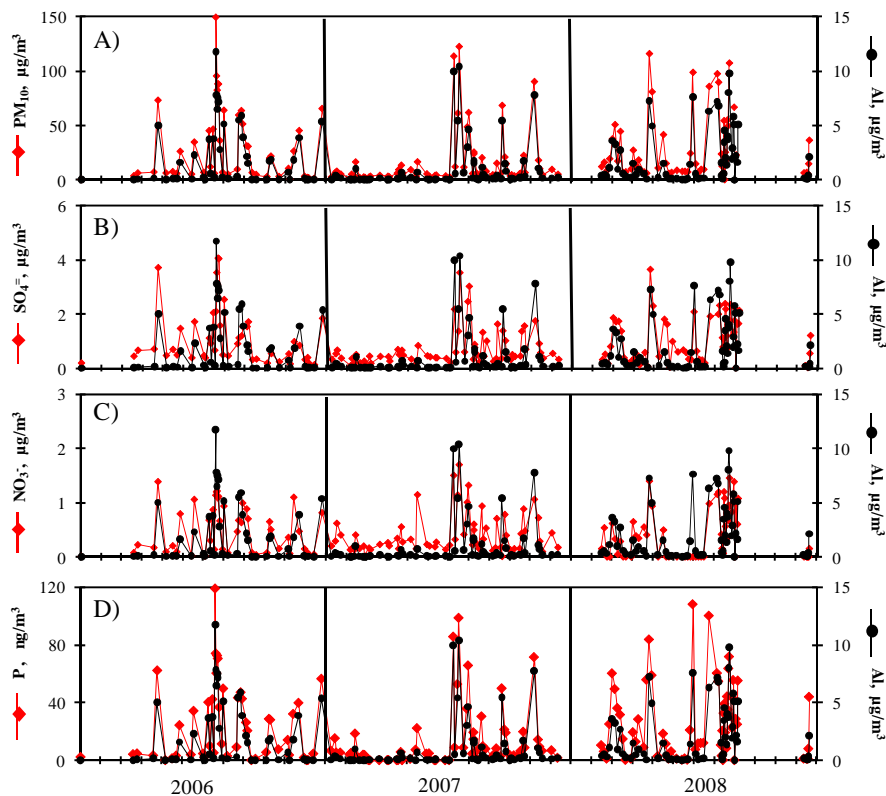


Fig. 3. Concentrations of PM_{10} , aluminium, sulphate and nitrate recorded at Izaña.

Title Page

Abstract

Introduction

Conclusions

References

Tables

Figures

◀

▶

◀

▶

Back

Close

Full Screen / Esc

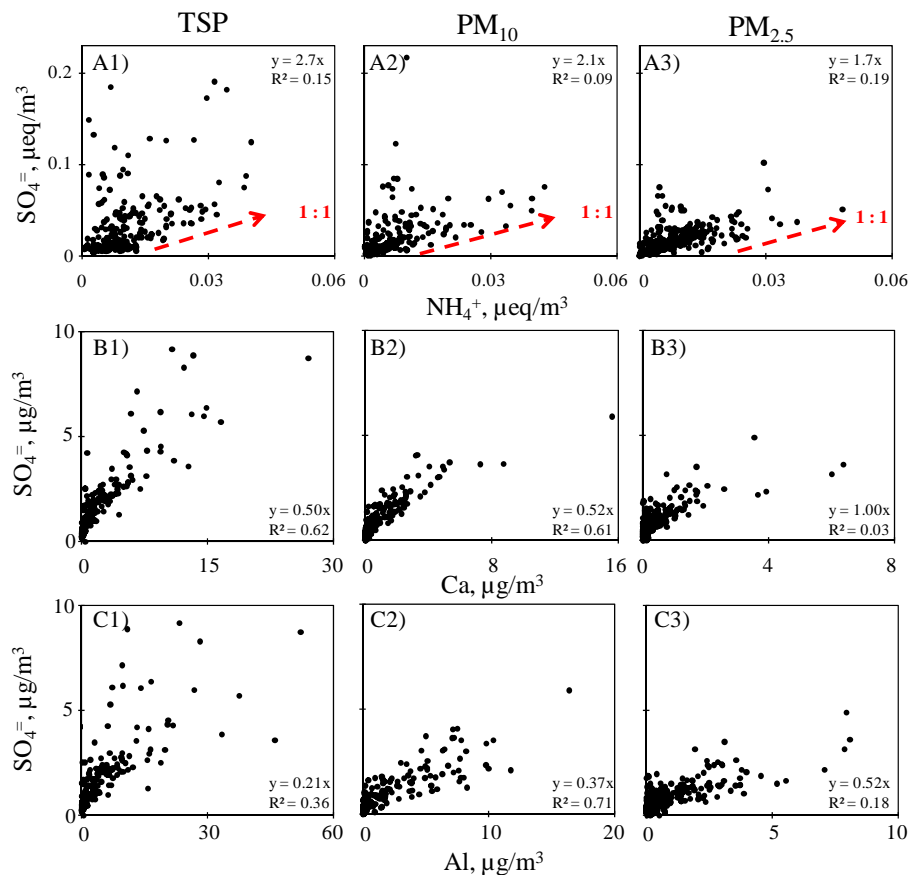
Printer-friendly Version

Interactive Discussion



Transport of dust and
pollutants mixings

S. Rodríguez et al.

**Fig. 4.** Concentrations of sulphate versus ammonium, calcium and aluminium.

Title Page

Abstract

Introduction

Conclusions

References

Tables

Figures

◀

▶

◀

▶

Back

Close

Full Screen / Esc

Printer-friendly Version

Interactive Discussion



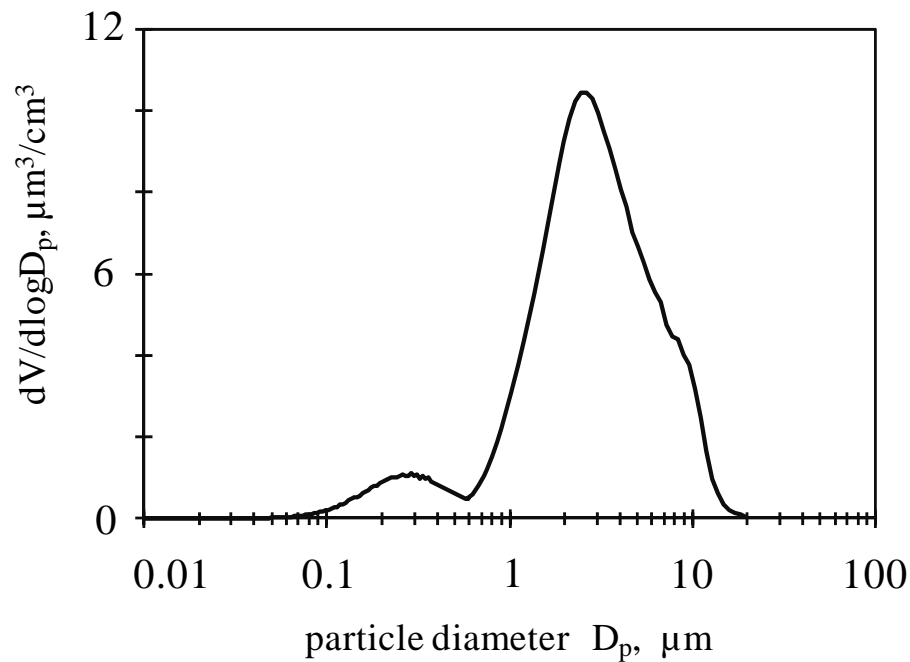


Fig. 5. Particle size distribution recorded at Izaña during Saharan dust events.

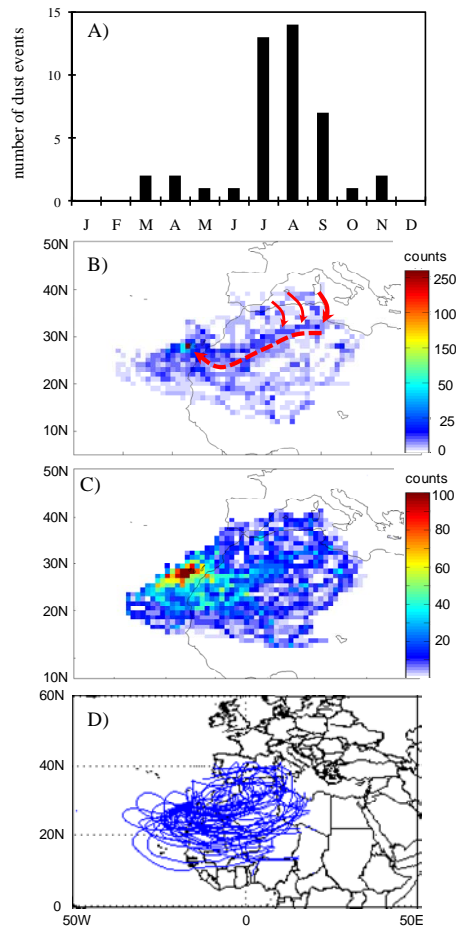


Fig. 6. (A) Number of events with dust concentrations $>10 \mu\text{m}^{-2}$ in PM_{10} . (B) and (C) Frequency of pass of trajectories by each 10×10 pixel scale set to maximum value (B) and set to 100 (C). (D) Set of trajectories included in the analysis of dust events in PM_{10} . Red line in (A) highlights the deduced transport pathway.

Transport of dust and
pollutants mixings

S. Rodríguez et al.

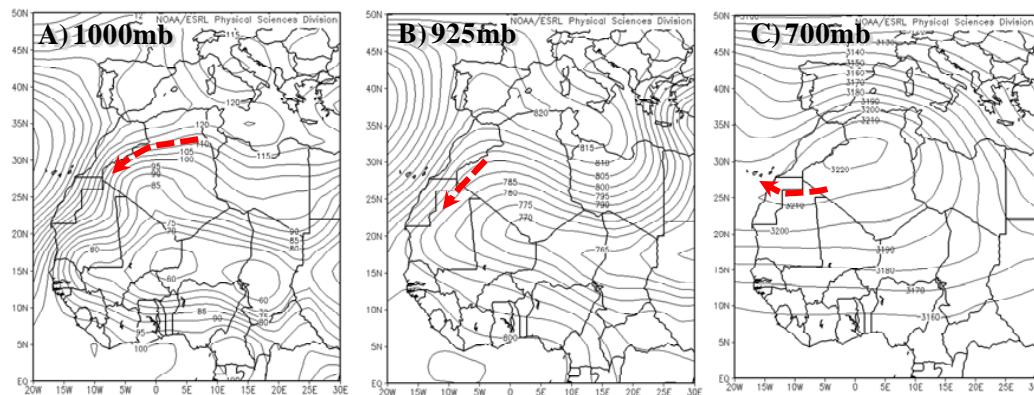


Fig. 7. Geopotential for 1000, 925 and 700 mb averaged during July and August. Red lines highlight the airflows involved in the transport pathways highlighted in Figure 6B.

Title Page

Abstract

Introduction

Conclusions

References

Tables

Figures

◀

▶

◀

▶

Back

Close

Full Screen / Esc

Printer-friendly Version

Interactive Discussion



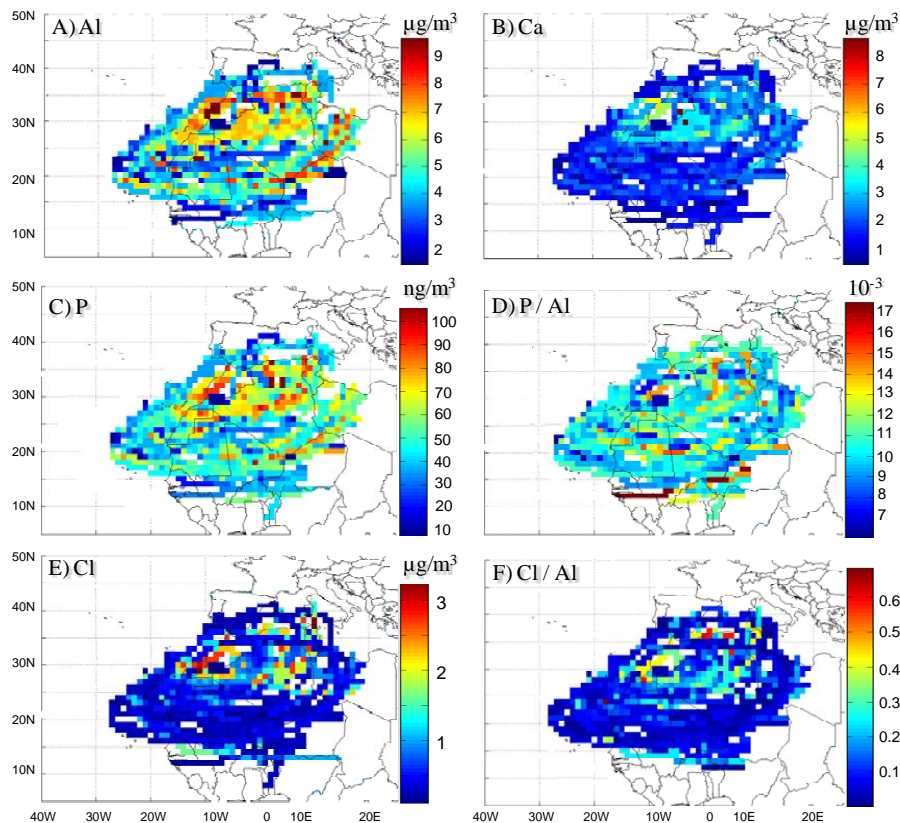


Fig. 8. Median concentrations at receptor (MCAR) plots for Al, Ca, P and Cl concentrations and for the P/Al and Cl/Al ratios in the PM₁₀ fraction.

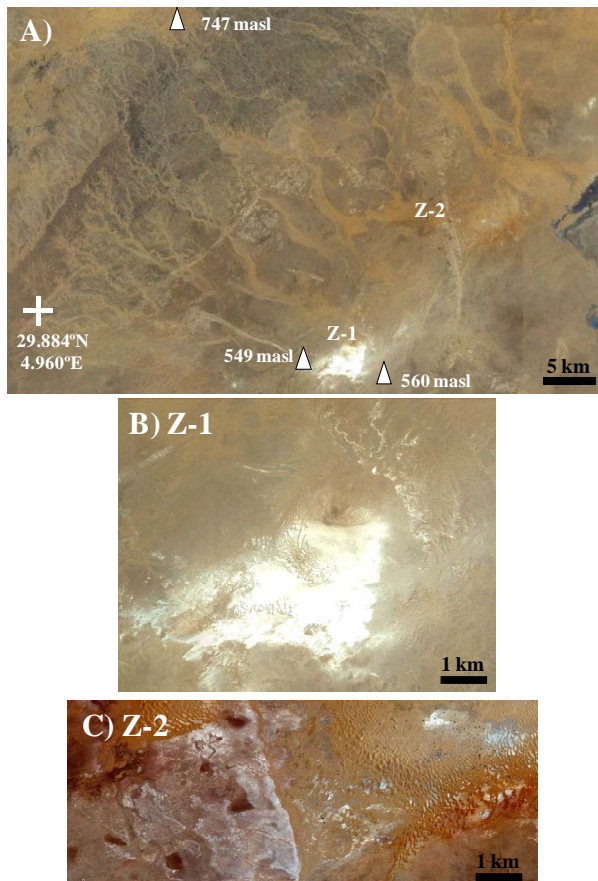


Fig. 9. Satellite view of a part of the Bechar province **(A)** and two zooms of the area **(B and C)**.

Transport of dust and
pollutants mixings

S. Rodríguez et al.

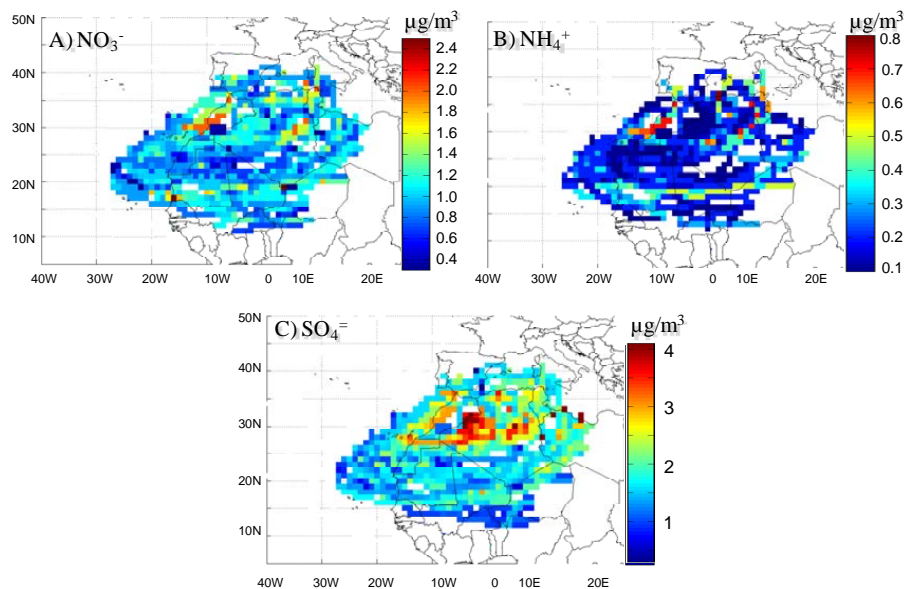


Fig. 10. Median concentrations at receptor (MCAR) plots for nitrate, ammonium and sulphate concentrations in the PM₁₀ fraction.

[Title Page](#)[Abstract](#)[Introduction](#)[Conclusions](#)[References](#)[Tables](#)[Figures](#)[◀](#)[▶](#)[◀](#)[▶](#)[Back](#)[Close](#)[Full Screen / Esc](#)[Printer-friendly Version](#)[Interactive Discussion](#)

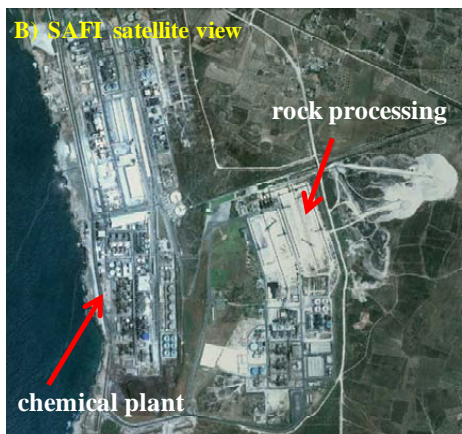


Fig. 11. Pictures of SAFI phosphate/fertilizer industry (**A**, **B**) and Benguerir/Yousoufia phosphate mine (**C**) in Morocco.

Transport of dust and pollutants mixings

S. Rodríguez et al.

Title Page

Abstract

Introduction

Conclusions

References

Tables

Figures

◀

▶

◀

▶

Back

Close

Full Screen / Esc

Printer-friendly Version

Interactive Discussion



Transport of dust and pollutants mixings

S. Rodríguez et al.



Fig. 12. (A) Ouargla basin (red circles indicate the location of certain chots), (B) in situ picture of Chott Oum El Raned, (C–E) in situ pictures of Hassi Mesahoud.

Title Page	
Abstract	Introduction
Conclusions	References
Tables	Figures
◀	▶
◀	▶
Back	Close
Full Screen / Esc	
Printer-friendly Version	
Interactive Discussion	



Transport of dust and pollutants mixings

S. Rodríguez et al.

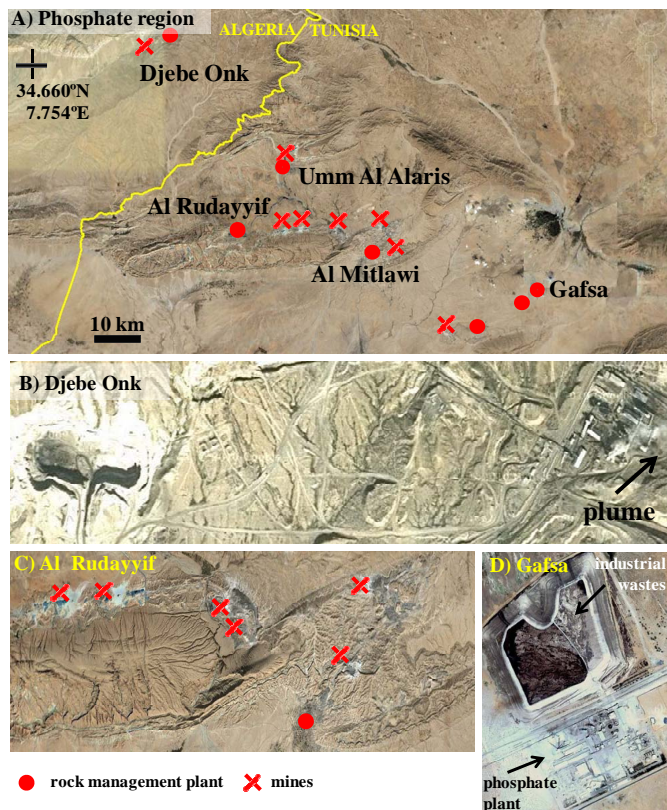


Fig. 13. (A) Satellite view of the phosphate mines region in the border of Algeria (Tébessa province) and Tunisia (Gafsa province). A zoom is shown for Djebe Onk phosphate mines (B), Al Rudayyif (C) and Gafsa (D) mines.

Title Page

Abstract

Introduction

Conclusions

References

Tables

Figures

◀

▶

◀

▶

Back

Close

Full Screen / Esc

Printer-friendly Version

Interactive Discussion



Transport of dust and
pollutants mixings

S. Rodríguez et al.

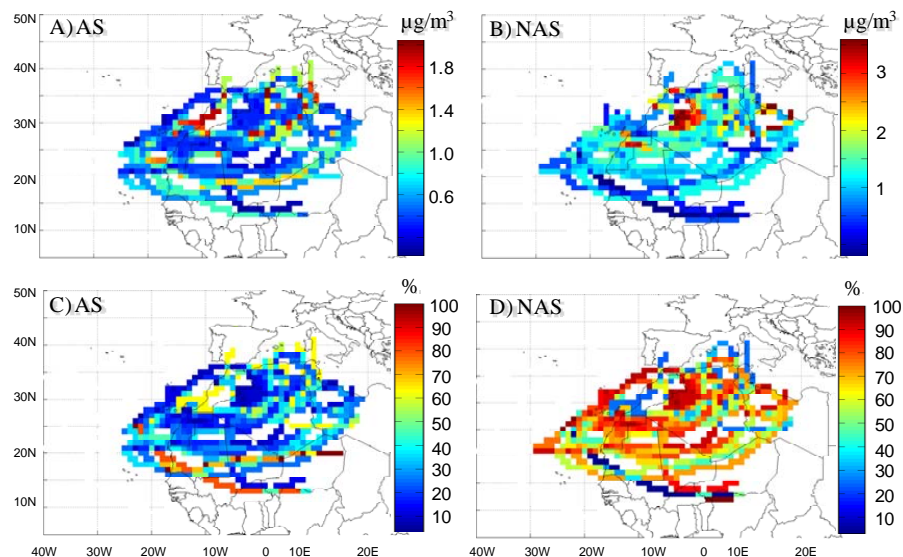


Fig. 14. Median concentrations at receptor (MCAR) plots for ammonium sulphate (AS) and non-ammonium sulphate (NAS), in the PM₁₀ fraction, in terms of absolute concentration (A–B) and contribution to total sulphate (C–D).

[Title Page](#)[Abstract](#)[Introduction](#)[Conclusions](#)[References](#)[Tables](#)[Figures](#)[◀](#)[▶](#)[◀](#)[▶](#)[Back](#)[Close](#)[Full Screen / Esc](#)[Printer-friendly Version](#)[Interactive Discussion](#)

Transport of dust and pollutants mixings

S. Rodríguez et al.

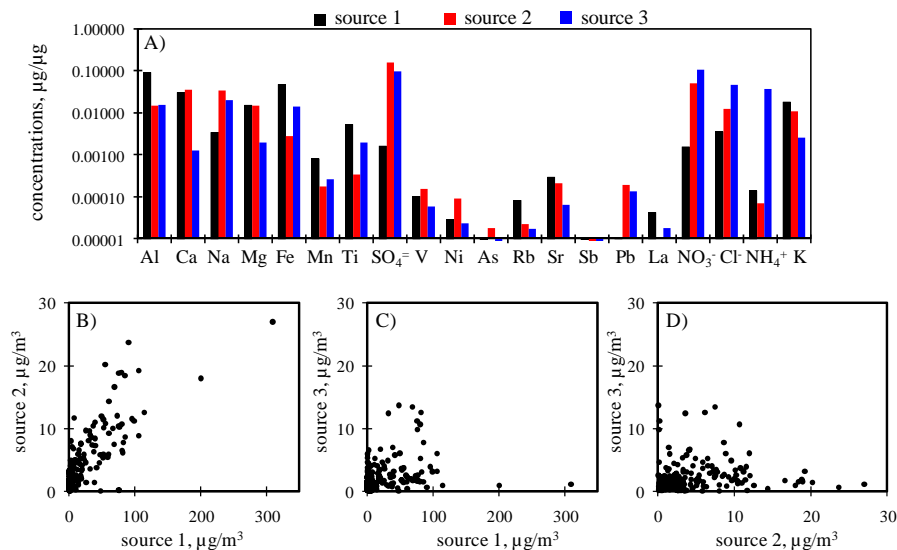


Fig. 15. Chemical profile (A) and contributions (B–D) obtained by applying the PMF2 model to the PM₁₀ composition at Izaña.

Title Page

Abstract

Introduction

Conclusions

References

Tables

Figures

◀

▶

◀

▶

Back

Close

Full Screen / Esc

Printer-friendly Version

Interactive Discussion

